Edited by
Tetyana Baydyk

ENERGY SYSTEMS AND RESOURCES: OPTIMISATION AND RATIONAL USE

Collective monograph

Technology® Center

2024

UDC 621.311
E54

Published in 2024
by TECHNOLOGY CENTER PC®
Shatylova dacha str., 4, Kharkiv, Ukraine, 61165

E54

Authors:
Edited by **Tetyana Baydyk**
Maksym Kovzel, Olga Nosko, Tetyana Baydyk, Masuma Mammadova, Ernst Kussul, Airam Curtidor, Yurii Sniezhkin, Zhanna Petrova, Vadym Paziuk, Viacheslav Mykhailyk, Tetiana Korinchevska, Kateryna Samoilenko, Igor Kozlov, Vyacheslav Kovalchuk, Viacheslav Miliev, Mykola Holovin, Serhii Vistiak, Olexiy Kozlov, Natalia Dunaievska, Taras Shchudlo, Ihor Beztsennyi, Dmytro Bondzyk, Yevhen Miroshnychenko
Energy systems and resources: optimisation and rational use: collective monograph. – Kharkiv: TECHNOLOGY CENTER PC, 2024. – 192 p.

This monograph is a complex scientific and applied work covering the most important directions in the field of sustainable energy, materials science and environmental safety. The studies and recommendations presented in it have practical significance and can be used for further development of scientific and technological solutions in this field.
The results presented in the monograph can be useful in the development of new solutions for the energy industry, in the design of renewable energy systems, in the sphere of waste utilisation and in the issues of reducing the environmental impact of industrial facilities. The obtained data and recommendations are intended for a wide range of specialists, including engineers, developers, scientists, designers, as well as undergraduate and postgraduate students of technical areas of training.
Figures 88, Tables 41, References 147 items.

DOI: 10.15587/978-617-8360-02-3
ISBN 978-617-8360-02-3 (on-line)

Cite as: Baydyk, T. (Ed.) (2024). Energy systems and resources: optimisation and rational use. Kharkiv: TECHNOLOGY CENTER PC, 192. doi: http://doi.org/10.15587/978-617-8360-02-3

9 786178 360023

AUTHORS

CHAPTER 1

MAKSYM KOVZEL
PhD, Associate Professor, Forensic Expert
Dnipropetrovsk Scientific Research Forensic Center of the MIA of Ukraine
ORCID: https://orcid.org/0000-0001-5720-1186

OLGA NOSKO
PhD, Associate Professor, Dean
Faculty of Quality and Material Engineering
Institute of Industrial and Business Technologies Ukrainian State University of Science and Technologies
ORCID: https://orcid.org/0000-0002-5749-7578

CHAPTER 2

TETYANA BAYDYK
Doctor of Technical Sciences, Professor,
Investigator Titular C
Department of Micro and Nanotechnology
Institute of Applied Sciences and Technology
National Autonomous University of Mexico
ORCID: https://orcid.org/0000-0002-3095-2032

MASUMA MAMMADOVA
Doctor of Technical Sciences, Professor, Head of Department
Department of Number 11
Institute of Information Technologies
ORCID: https://orcid.org/0000-0002-2205-1023

ERNST KUSSUL
Doctor of Technical Sciences, Professor,
Investigator Titular C, Head of Group
Department of Micro and Nanotechnology
Institute of Applied Sciences and Technology
National Autonomous University of Mexico
ORCID: https://orcid.org/0000-0002-2849-2532

AIRAM CURTIDOR
Department of Micro and Nanotechnology
Institute of Applied Sciences and Technology
National Autonomous University of Mexico
ORCID: https://orcid.org/0000-0002-7388-1385

CHAPTER 3

YURII SNIEZHKIN
Doctor of Technical Sciences, Professor, Acting Head of the Institute, Academician of NAS of Ukraine
Institute of Engineering Thermophysics of NAS of Ukraine
ORCID: https://orcid.org/0000-0002-9049-3392

ZHANNA PETROVA
Doctor of Technical Sciences, Senior Researcher
Department of Mass Transfer in Heat Technologies
Institute of Engineering Thermophysics of NAS of Ukraine
ORCID: https://orcid.org/0000-0001-7385-8495

VADYM PAZIUK
Doctor of Technical Sciences, Associate Professor
Department of Mass Transfer in Heat Technologies
Institute of Engineering Thermophysics of NAS of Ukraine
ORCID: https://orcid.org/0000-0002-4955-1941

VIACHESLAV MYKHAILYK
PhD, Senior Researcher
Department of Mass Transfer in Heat Technologies
Institute of Engineering Thermophysics of NAS of Ukraine
https://orcid.org/0000-0003-2712-1382

TETIANA KORINCHEVSKA
PhD, Senior Researcher
Department of Mass Transfer in Heat Technologies
Institute of Engineering Thermophysics of NAS of Ukraine
ORCID: https://orcid.org/0000-0002-6638-4743

KATERYNA SAMOILENKO
PhD, Senior Researcher
Department of Mass Transfer in Heat Technologies
Institute of Engineering Thermophysics of NAS of Ukraine
ORCID: https://orcid.org/0000-0002-5169-4466

CHAPTER 4

IGOR KOZLOV
Doctor of Technical Sciences, Professor
Department of Nuclear Power Plants
Odesa Polytechnic National University
ORCID: https://orcid.org/0000-0003-0435-6373

CONTENTS

LIST OF TABLES

LIST OF FIGURES

INTRODUCTION

Modern global challenges in the field of energy, ecology and resource conservation require a systematic approach and search for innovative solutions aimed at improving energy efficiency, introduction of renewable energy sources and rational use of natural resources. The rapid depletion of traditional fuels such as coal, oil and gas leads to the need to develop new technologies that ensure stable energy supply with minimal environmental impact. In addition, increasing volumes of industrial and domestic waste, as well as increasingly stringent environmental requirements for enterprises, create additional challenges for the energy sector and industry as a whole.

In this regard, studies aimed at developing new materials, technologies and approaches to the organisation of energy systems that could ensure high efficiency and environmental safety are becoming relevant. This monograph is devoted to a comprehensive study of some of the most important areas in the field of materials science, alternative energy and sustainable development, which are of strategic importance for modern industry and energy.

The following key issues are discussed in detail in the monograph:

– the influence of a magnetic field on the microstructure of silicon grown by the Czochralsky method (Cz-Si) doped with the elements Al, Mg, Cu, Fe, Zr, and Hf. For the first time in scientific practice the study of structural changes of silicon under the influence of magnetic field and the influence of various impurities on its crystal lattice is carried out. The research shows that these elements differently affect the interaction energy of silicon atoms in the lattice and behave differently under the influence of a magnetic field. The results may be useful for the production of semiconductor materials with improved characteristics, which is critical for microelectronics and solar energy;

– development of innovative designs of solar concentrators. The work explores the issues of improving the technological efficiency and reducing the production cost of solar concentrators, which plays a key role in the development of alternative energy. The existing designs have been analysed and new solutions have been proposed, aimed at reducing the weight of structural elements, reducing assembly costs and increasing the ease of operation. The developed prototypes of solar concentrators can be widely applied in agriculture, in power supply systems of residential buildings and in organic waste recycling processes;

– utilisation of municipal solid waste (MSW) in the energy balance of Ukraine. One of the most important directions of sustainable development is the processing and utilisation of waste for its further use as an alternative energy source. In this paper the physical and chemical properties of RDF (refuse-derived fuel) - an alternative solid fuel produced from combustible components of MSW are investigated. The kinetics of drying, thermal decomposition and calorific value of RDF of different compositions were analysed. The obtained data can contribute to the development of energy-efficient technologies of RDF production and its effective application at thermal power plants;

– analysis of the state and prospects of development of the energy complex of Ukraine. An important part of the monograph is the analysis of the structure of the energy balance of the country, identification of key problems and proposals to improve the current situation. The issues of using traditional energy resources, such as coal, oil, gas and nuclear fuel, as well as the prospects of transition to renewable energy sources are considered. A methodology for selecting optimal energy strategies for different regions, taking into account environmental and economic factors, is propose;

– co-firing of coal and biomass as a way to reduce harmful emissions. The work is aimed at the development of coal and biomass co-combustion technologies, which allows to reduce CO_2, SO_2 and NOx emissions, diversify fuel sources and increase the sustainability of energy systems. The basic principles of co-combustion are investigated, heat engineering calculations are performed, and experiments on co-combustion of gas coal and biomass are carried out. Recommendations for the introduction of technologies at TPPs have been developed, which can contribute to the improvement of energy efficiency and environmental safety.

Modern methods and approaches, including X-ray diffraction analysis, thermogravimetric analysis, computer modelling in ANSYS FLUENT software packages, as well as experimental methods of measuring and controlling the characteristics of materials were used in the research within the framework of this work.

The results presented in the monograph can be useful in the development of new solutions for the energy industry, in the design of renewable energy systems, in the sphere of waste utilisation and in the issues of reducing the environmental impact of industrial facilities. The obtained data and recommendations are intended for a wide range of specialists, including engineers, developers, scientists, designers, as well as undergraduate and postgraduate students of technical areas of training.

Thus, this monograph is a complex scientific and applied work covering the most important directions in the field of sustainable energy, materials science and environmental safety. The studies and recommendations presented in it have practical significance and can be used for further development of scientific and technological solutions in this field.

DOI: 10.15587/978-617-8360-02-3.CH1

Maksym Kovzel, Olga Nosko

CHAPTER 1

MAGNETIC TREATMENT OF SEMICONDUCTOR SILICON

ABSTRACT

The current publication reports on the magnetic field influence on the microstructure of Cz-Si doped with Al, Mg, Cu, Fe, Zr, Hf. The point is that these dopants have different effects on the interaction energy of silicon atoms in its crystal lattice and differently behave under magnetic field treatment. In this context, the problem of silicon processing is first time addressed.

It is established that the dopants (Al, Mg, Cu, Fe), which decrease the energy of atom interaction within the crystal lattice of silicon, lead to the increase in the defects of the silicon structural units after 240 hours of magnetic field treatment while 720 hours produce the decrease in the quantity of such defects.

Cz-Si doped with Zr, Hf (these dopants increase the interaction energy of the silicon crystal lattice) experiences the decrease in the quantity of defects in the structural units starting from 240 of exposing to the magnetic field.

By means of X-ray diffraction technique, the occurrence of new peaks on the scattering angles of 90–92 degrees has been detected, that is due to Si_{FCC} lattice distortion and the formation of Si orthorhomic alongside with it. This indicates phase transformations in the samples of semiconductor silicon during magnetic treatment at room temperature.

KEYWORDS

Semiconductor silicon, complex doping, interaction energy, phase transformations, dislocation density, twins, magnetic field treatment, microhardness, specific electrical resistivity, charge minority-carrier lifetime.

Commonly, power engineering for energy production has always been posed as the principle industry of any developed country. To provide energy independence is one of the strategic tasks to address in modern Ukraine's economy development. The promising way how this task can be solved is in maximizing the strategic balance by enhancing the energy share from the own energy

resources. The urgency of this problem in Ukraine determines the need for the development of the alternative energy forms based on renewable sources alongside with the energy saving.

Back in 1990, the world's developed countries initiated transition stage to the new energy sources. The environmentally-friendly attitude is among the features of this stage, i.e. it strives to reduce environmental pollution and to minimize carbon dioxide and sulfur dioxide emissions. Expected that during the next two or three decades, the mankind is to introduce ecologically-friendly renewable energy sources into everyday life, primarily wind power and solar power. Ignoring these tendencies threats with ecological disasters of the future and is able make the entire life on earth endangered.

Moreover, pursuing the target of achieving European Integration, Ukraine sets the strategic goal of rapid implementation for the energy produced from the renewable energy sources. Thus, solar power is the most promising direction of such kind in Ukraine, where there is a high potential due to the country's geographical position in the terrestrial latitudes with good solar radiation intensity. The latter implies that the photovoltaic equipment can be used throughout the year. Further, the high-performance operating time in the northern areas makes up 5 months (May to September), while in the southern areas it is 7 months (April to October). However, the solar power economic features require careful further study. According to experts, the operating cost of the electrical power generated by the solar modules will reduce by 5 times during the next 10 or 15 years.

Taking into account the above stated necessity of solar engineering development, silicon, as a constituent of solar cells, draws the close attention of the scientists. In particular, thermal stability of silicon crystal properties is one of the basic parameters of semiconductor quality and at the same time it is the very factor that determines the resistance of microelectronic devices to degradation at elevated temperatures and expands the area of their operation. Furthermore, thermal stability of silicon crystals is essential for manufacturing microelectronic devices, since crystals are exposed to high temperatures in many technological processes that often irretrievably deteriorate properties of primary crystals.

The topical character of the study is determined by the need to reveal the degradation regularities in silicon physical properties and the means of their further control, as well as by the necessity to develop semiconductor devices based on silicon with stable parameters.

The manufacturing processes and operation of semiconductor devices are known to be followed by thermal and radiation effects that cause the changes in the physical properties of both in semiconductors and the devices based on them. However, there are rigorous specifications to the manufactured semiconductor devices concerning stability of their parameters under various radiation and thermal operating conditions. The potentially productive ways of control over silicon physical parameter degradation are in its thermal treatment, doping and processing within a magnetic field. Today there is a growing demand for monocrystalline silicon for photo-emissive converters from both foreign and domestic companies. The circle of scientific interests of the global research community continues to be focused on solar cell manufacturing techniques from cheap silicon that can be represented by polycrystalline silicon of low-purity ("dirty"), thin films of amorphous silicon of polycrystalline type and other semiconductors.

Considering the full-scale opportunities for the silicon and the dedicated equipment, the need for the sufficiently high level of readiness should be provided, which enables the rapid and efficient growth of modern solar power in Ukraine.

The first section of the current publication contains the literature review on the regularities in semiconductor silicon structure formation and properties, as well as the modern views and opinions on phase transformations and martensitic transformation mechanisms that occur in semiconductor silicon. The contemporary publications targeting the problem of the magnetic field effect on the semiconductor silicon structure and properties have been reviewed. This analysis enables outlining the character of the further studies and the stages of the topical scientific and technical task to be solved for the current research: for the present publication we set the task to develop the complex resource-saving technology and energy saving solution for production of semiconductor silicon with enhanced physical and mechanical properties by influencing its liquid and solid forms physically and chemically with the objective to expand the areas of its application.

The second section provides the data on the material and the research techniques. The object of the research is monocrystalline semiconductor silicon samples (Cz-Si) grown by Czochralski method, both in undoped version and doped with single elements of B, Sn, Ge, Hf, Zr, and with the complexes of B-Sn and B-Mo, ranging from $2 \cdot 10^{-4}$ to $8.7 \cdot 10^{-2}$ at % in the initial state, after they have been exposed to the complete heating-cooling cycle, the thermal treatment regimes and the weak direct current magnetic field effect.

In the third section the structure peculiarities formed under the magnetic field effect for both the undoped Cz-Si samples and the Cz-Si doped with Al, Mg, Cu, Fe, Zr, and Hf have been analysed, with the focus on the difference in the dopant effects on the silicon atom interaction energy within silicon crystal lattice. During the magnetic treatment at room temperature, the phase transformations have been detected in semiconductor silicon samples via X-ray diffraction technique.

In the fourth section we report on the magnetic treatment effect on the microhardness values of doped Cz-Si structural units.

The fifth section reveals physical parameters and mechanical properties of the doped and undoped silicon samples before and after magnetic field treatment with the induction of 66 mT.

1.1 EARLIER RESEARCH FINDINGS AND RELEVANT LITERATURE REVIEW

1.1.1 CRYSTALLOCHEMICAL PECULIARITIES OF SEMICONDUCTOR SILICON

Silicon is an element of IVB subgroup of the periodic system, the atomic number of 14, an electron configuration of $1S^2 2S^2 P^6 3S^2 P^2$. Silicon atoms possess four valence electrons and form a diamond-type or a zinc blende type of the crystal lattice with covalent bonds and coordination number of 4 at room temperature, when silicon behaves as a typical semiconductor.

Silicon has high specific melting point and its density increases when transformed from a solid state to a liquid one [1].

Under atmospheric pressure silicon is a covalent substance with strong semiconductor properties. Interatomic bonds are defined by means of tetrahedral symmetry and have sp^3 hybrid composition. All 4 silicon atom bonds are equivalent and equally saturated.

In [1–3], it is shown that silicon undergoes the semiconductor-metal transition during melting, while at high pressure (~12 hPa) [2] there has been detected the transition from purely covalent structure (K=4) of a diamond to bcc tetragonal covalent metal structure within silicon (as the white tin type) and then (~16 hPa) the transition to the typical body-centered cubic metallic structure (K=8).

The publications [1–4] suggest that the transition to metallic state (when melting the elements belonging to IVB group (germanium and silicon) as well as compounds of AIIIBV and AIIBIV types etc.) is related to the disruption in homopolar bond space system and to the separation of many free electrons; the latter form a new configuration with electron density of higher symmetry [3].

Silicon melting causes the sharp increase in its conductivity which value becomes equal to the liquid metal conductivity value. It should be noted, that conductivity alteration is connected to the rearrangement from the "diamond structure" of a solid state to denser packing peculiar to the "metallic state" that occurs when melting these substances of short range ordering; this process is confirmed by the density increase factor that to some extent reflects the structural changes. According to the X-ray investigation data, it has been proved that the structure change occurs in many semiconductors with diamond structure (including silicon) when in a liquid state. During melting silicon coordination number increases from 4 to 6.

1.1.2 PHASE TRANSFORMATIONS IN SEMICONDUCTOR SILICON

It is peculiar of silicon to have high specific fusion heat as well as density increase during transition from a solid state to a liquid state [5, 6]. Fusion entropy of silicon is considerably higher than that of pure metals that is why its value is greatly affected by the process related to the electron delocalization at the solid-liquid transition. The electron component is connected to the chemical bond type change (mainly from covalent bonds to metallic ones) during melting that is followed by the marked increase of free electron concentration [6].

For the substances that become highly metallized at melting, solid-liquid transition is followed by disruption in the sp^3-hybrid homopolar bond space system, by detachment of four valence electrons and their transition to the free state and by major changes of the short range ordering and atom vibrational spectrum [7–9].

A distinguishing feature of the first-order phase transitions in silicon (by that we mean melting and crystallization) is the change of the free electron number and the important role of the electron component is in this transition. Apparently, at the temperature and the pressure change, allotropic transformation can be followed by the free electron number alteration.

The data on phase transitions in the solid polymorphic type of silicon are given in the publications [6–8]. Polymorphic closely-packed metallized modifications of silicon are formed at high pressure [7]. At the pressure of 12 hPa and the temperature of 20 °C, the phase transition SiI→SiII has been detected by means of resistometric investigation and X-ray analysis [8]. A notable dependence has been revealed for the SiI→SiII phase transition on the shift components of load, pressure and the holding-pressure time of the sample. Due to this, the transition continues at 2–3 hPa. SiII phase is reported as one having metallic conductivity. The inverse transition SiII→SiI has not been detected.

After subjecting SiII samples to certain pressure, there have been revealed 2 modifications of Si (SiIII and SiIV) by X-ray analysis under atmospheric conditions. Heating SiIII within 200–600 °C causes its lattice rearrangement and, consequently, there occurs SiIV modification with the hexagonal wurtzite-type structure. Under additional pressures, SiIV behaves as a metastable phase. Two assumptions have been suggested concerning SiIII: it either can be a stable phase under 12 hPa at 20 °C with a body-centered cubic lattice, or it is a transition phase from SiII of tetragonal structure when pressure is removed. Under the pressure of 12 hPa, SiII phase transforms into superconductive state if $T=6.7$ K [11].

In [9–11], the temperature dependence of some semiconductor silicon properties has been described, particularly, thermal expansion coefficient, hardness, lattice parameter, electrical properties at atmospheric pressure in the range from $T=20$ °C to $T<T_{melting}$. During phase transitions, semiconductor silicon undergoes discontinuous change of thermal, volumetric, mechanical and electrical properties due to the transition from one crystalline state into another. Establishing the property-temperature and property-pressure dependences allows revealing phase transition.

Normally, phase transition develops with a high rate, however, this behaviour is true only for certain regions. Being conditioned by the size and the number of a new phase regions that are formed per unit time, the volume rate of transformation is low in many cases, though the region formation rate is very high.

The volume rate of the transformation is taken into account in [9] for the studies on temperature dependence in silicon properties when heated at the rate of ≤5 °C/min. These studies on semiconductor silicon properties reveal the monotonic dependence.

The abnormal character of the temperature dependence of the sample linear dimensions shows that there are different silicon phases at certain temperatures due to formation of which the registered changes occur.

In [10], the following phase transitions in silicon at heating are described. The general conclusion based on the ultrapure silicon research data is that these phase transitions can be observed in the local crystal volumes during heating with the rate of less than 5 °C/min:

(I) within 250–350 °C $Si_{FCC}\rightarrow Si_{ORTHORHOMBIC}$;

(II) within 680–700 °C $Si_{ORTHORHOMBIC}\rightarrow Si_{BCC}$;

(III) within 1150–1200 °C $Si_{BCC}\rightarrow Si_{HCP}$;

(IV) within 1420 °C $Si_{HCP}\rightarrow P$.

Low-temperature transformations (I and II) have low ΔH values and can be referred as phase transitions that cause lattice atom shears at small distances. In this case we observe shear transformations that are based on the ordered lattice rearrangement. The lattices of both modifications are combined or adjacent while the shear transition starts heterogeneously. The nuclei appear in the areas with the dedicated dislocation nodes (the order growth rate is 10^3 m/sec). Polymorphic transformation rate is especially high in defect-free crystals. Phase transition III is accompanied by high thermal effect, so hyperthermal transformation in silicon is a first-order phase transition and it occurs due to the total rearrangement of the lattice. The specific feature of a first-order phase transition is the presence of interfaces that is why the transitions of this type lead to the fundamental crystal structure rearrangement.

The calorimetric analysis of the ultrapure semiconductor silicon [11] reveals that the phase transition is blurred and this phenomenon can be explained by as below:

– formation of polymorphic modifications with closely adjacent lattices;

– irregular distribution of impurity atoms within the crystals, namely O_2, H_2, C;

– irregular distribution of defects.

Considering the above stated, it can be suggested that when heating semiconductor silicon, its crystal lattice is proved to become denser before $T_{melting}$, conditioned by the degree of bond directions and followed by the transition to the metallic state. The transition of covalent crystals to the metallic state can be obtained regardless of the lattice disruption type and the techniques to influence the crystals.

The transition mechanism of the covalent crystals to the metallic state at various ways of the lattice excitement is the same: there occurs electron subcrystalline structure alteration, particularly, the sp^3-hybrid bond disruption is followed by the band gap narrowing and the corresponding increase in the number of charge carriers [11, 12].

The transition from the covalent bonding to the metallic one is carried out due to electron motion from the "coupled" state in the valance band to the "antibonding" conduction band, that leads to the decrease in the shear resistance of diamond lattice [12].

The experiment shows that at heating semiconductors, the transition from the semiconductor to the metal begins at the temperature considerably lower than $T_{smelting}$. It is interesting to note, that this temperature is not the same for the crystals obtained by different techniques [13]. The transition occurs due to the sequential lattice rearrangement from less dense to denser by the shear or shear-diffusion mechanism and is followed by the change in the correlation between the covalent component and the metal component of the chemical bond. In other words, in silicon there occurs direct and reverse martensitic transformation on its exposure to the different factors.

The most important feature of the diffusionless transformations is the concerted migration of large atomic groups during the new phase crystal growth. According to Kurdyumov, "Martensitic transformation is a regular lattice rearrangement in which the adjacent atoms do not interchange their places but only shear relative to each other at a distance which does not exceed the interatomic one" [14].

All the martensitic transformations without any exception have certain features conditioned by the following:

1) the cooperative character of atom migration during the crystal growth;

2) transformations in anisotropic elastic medium.

The crystals of the martensitic phase appear and reach their finite sizes at small-time intervals. The increase in the amounts of new phases takes place mainly due to the formation of new crystals, however, in some alloys there can be observed discontinuous growth of previously formed plates. The martensite crystals usually have a shape of a double convex lens and are twinned formations with a twining plane that coincides with the lens symmetry plane. Similar to twinning, such martensite crystal shape is explained by the elastic strain effect that occurs in the surrounding matrix during the growth of the new phase crystals.Theoretically, the analogy between twinning and diffusionless transformations is so due, that many authors regard twinning as a special case of diffusionless transformation during which the substance structure remains unchanged [15, 16]. Twinning can occur both with the change of the shape and without it (for instance, quartz). By analogy, diffusionless phase transformations can be subdivided into two groups:

1) diffusionless phase transformations that change the shape;

2) diffusionless phase transformations that do not lead to the change of the shape.

The transformation accompanied by the shape change is the one, during which there occurs primary macroscopic deformation; the transformation without such a change in the shape is the one, at which there is only "secondary" deformation. Thus, martensitic transformations are the diffusionless transformations accompanied by shape change. The diffusionless transformations with no shape change are more common for the crystals with complex structure, chiefly, for molecular crystals. These transformations, in case of preserving the atom migration cooperative character, can be deprived of many peculiar to martensitic transformations features related to the shape change.

In combination with the elastic medium effect on the growing crystal, the macroscopic shear, that follows martensitic transformations, causes the "elastic" martensite crystal formation. This phenomenon is analogous to elastic twinning. The martensite crystal growth takes place due to regular atom migration to new dislocations, so that the adjacent atoms of the initial lattice remain adjacent in the new lattice as well. On the separation interface of the two phases, there is one lattice which continuously transforms into the other, i.e. there is a coherent bonding between the lattices of the initial phase and the new one. With the crystal size increase, the elastic strains on the interface surface of the two phases also increase; eventually, these strains lead to plastic deformation and, consequently, to coherence violation between the two lattices and the crystal growth character alteration.

When covalent crystals are heated to the critical values at certain temperature due to the increase in the antiphase oscillation amplitude, there occurs covalent bond breakdown and the localized pairs of electrons in them become collective, that, in its turn, predetermines transition to the metallic state.

The transition of covalent crystals to the metallic state can be achieved irrespectively to the lattice excitement and the techniques of influence to which the crystal is exposed to: heating, high laser irradiation, radiation and magnetic exposure, high pressure, explosive treatment, etc.

Moreover, the mechanism of the covalent crystal transition to the metallic state is the same whatever the techniques of the lattice excitement: electron subcrystalline structure changes, namely the sp^3-hybrid bond disruption is followed by the band gap narrowing and, consequently, by the increase in the charge carriers quantity [17, 18]. The concentration of the charge carriers in InSb solid phase even at the temperature of ~420 °C reaches $0.3 \cdot 10^{21}$ cm^{-3} while in InSb liquid phase at $T_{melting}$ it is $N_t = 5 \cdot 10^{21}$ cm^{-3} [18]. The same results have been obtained in [17] for semiconductor silicon: $N_t = 1.0 \cdot 10^{25}$ cm^{-3} at the temperature of ~727 °C, that corresponds to metallic state.

The transition from the covalent bonding to the metallic one takes place due to transferring of electrons from the "coupled state" in "antibonding" conductive area, that leads to the decrease in the shear resistance of the diamond lattice [19].

The problem of heating which initiates the transition of semiconductor into metal starting at the temperature much lower than the melting temperature (different for different crystals) [13] is relevant to [17, 18] and finds its further explanation as given below. The gradual rearrangement of the lattice into the denser one by the shear or shear-diffusion mechanism is followed by the correlation change between the covalent and metal chemical bond components. For instance, in Si, Ge, and InSb crystals there occurs direct transformation or reverse martensitic transformation depending on the influence produced. According to the general regularities of semiconductor property changes within the range of 0.16–0.20 $T_{melting}$, the atoms in the crystal lattice interact via the covalent bond pattern while within 0.2–0.8 $T_{melting}$, heterodesmic covalent metal bonding occurs and eventually at the temperature higher than 0.8 $T_{melting}$ the metallic bonding is predominantly observed. The revealed regularity correlates with the idea of alteration of covalent crystal heat capacity at heating [20].

The classical theories tell that at the absolute zero of temperature, all atoms in the crystal are motionless and the potential energy of their interaction is minimal. At quite low temperatures atoms are supposed to have small oscillation, at that, the kinetic energy value of the atom oscillation should be small as compared to their interaction energy. With the temperature and oscillation amplitude increase, the atom interaction energy increases as well. At the temperature increase by 1 degree, the value of the oscillation energy absorbed determines the so called oscillating temperature, and, at first approximation, heat capacity (harmonious oscillator). However, when heated under conditions of constant pressure, the thermal expansion of a solid occurs during which the phenomenon grows into a more complicated character. The oscillation of the atom and its shift from the initial state of equilibrium generate the forces that affect the oscillation of the adjacent atoms. A small difference in a phase that can occur at any certain period of time leads to the fact that the atoms do not possess rigidly fixed middle positions to be independent of the adjacent atoms. Moreover, since all the interacting atoms of a solid body take part in the oscillating process, this process cannot have a single frequency. The general energy of the crystal does not change at a constant temperature,

but the energy of each atom changes chaotically in the course of time. Thus, when explaining the temperature drive of the heat capacity phenomenon at the elevated temperatures, one should take into account the higher (anharmonic) expansion terms of the potential energy decomposition by shearing.

1.1.3 MARTENSITIC TRANSFORMATION MECHANISMS IN SILICON

The first instance of martensitic transformation in Si was observed under influence of the compressive loads in the temperature range of 400–700 °C within the region of indentation trace left by the diamond indenter [21]. It was assumed that there are the possible mechanisms of martensitic transformations in silicon, particularly the formation of hexagonal diamond phase with cubic twinning. The martensitic transformation occurs because a structure becomes thermodynamically unstable [14]. It is usually followed by the change of the shape that is manifested through the emergence of narrow plates within the compressed matrix. Due to this, and also as a result of cooperative diffusionless reaction, the martensitic transformation sufficiently adds to the strain energy. Thus, in order to initiate the transformation of this kind, it is necessary to apply sufficient affecting forces. Such forces of the martensitic transformation provide the absence of diffusion processes and can be induced in two ways, namely by accelerated cooling and by high degree of strain. Considerable supercooling leads to the emergence of quite strong affecting forces.

The crystallography of martensitic transformation has macroscopic nature as it describes the crystallography before and after the transformation but not the further process of the latter.

Crossing of twins is the most characteristic model of martensitic transformation in Si. Each twin is formed based on the differences in the mobility of partial dislocations within Si. This phenomenon is conditioned by the difference in glissile activation energy for both head dislocations and partial dislocations of the split screw dislocation and it increases at higher temperature. According to this model, twinning in Si requires three factors as following:

– the presence of an axial segment of a screw dislocation,

– the effect of shear stress on a dislocation segment in a primary plane and a crossed plane,

– medium temperatures.

In monocrystal of Si, the martensitic transformation takes place within the temperature range of 250–700 °C. Direct and reverse martensitic transformation occur in Si and they depend on the nature of its properties when being exposed to heating and cooling, due to which there can be observed some kind of hysteresis of martensitic transformation temperature interval.

By the origin, five types of twins can be distinguished:

a) concretion at random collision;

b) parallel lamination of molecules on a twin nucleus;

c) deposit of molecules on a large crystal formed in a twinning position;

d) transition from one modification to the other;

e) due to mechanical action.

The more symmetric the crystal structure is, the less likely is the twin formation. In crystals with low symmetry, different types of twinning can occur. Apparently, the formation of various types of twins is due to the lattice symmetry decrease during $Si_{FCC} \rightarrow Si_{ORTHORHOMBIC}$ phase transformation within Si samples that have been exposed to thermal treatment in the temperature range of 250–550 °C. Twinning is hardly observed during thermal treatment in the region of coexistence of $Si_{FCC} \rightarrow Si_{BCC}$ (750 °C).

Only shear stresses can affect twinning. Twin boundary energy during twin formation is of secondary importance. As the crystal form preserves while twinning, small distortions can be observed in the transition section. This section has a structure similarity to that of the high-temperature modification, while the twin boundary movement resembles the movement of a phase boundary at polymorphic transformation. During the closed loop of polymorphic transformations in single crystals of pure substances, a regular crystallographic direction of high-temperature grain modification is preserved; the latter is formed respectively to the primary single crystal. Moreover, in the microstructure, the changes occur connected with the new grain growth that is the result of phase transformations [15, 22]. The grains have almost similar crystal-lattice orientation, and when exposed to X-ray diffraction technique, such aggregation reveals itself as a single crystal; the same process is observed when growing monocrystalline silicon [22].

Thus, the development of two-dimensional crystal boundaries in monocrystalline silicon and the presence of two-dimensional conductivity are related to the formation of the shear phase transitions and twin boundaries.

The martensitic crystal formation not only leads to the crystal lattice type change, but also to plastic deformation of both the new phase and the matrix. The plastic deformation develops due to the slip of twinning. Such redundant or accommodative deformation is an integral part of martensitic transformation and provides minimum energy of elastic distortion on the invariant surface of phase interfaces. The elastic resizing of the crystal can be observed under compressive stresses or tensile stresses. Similar to twinning, the formation of martensitic crystals may be caused by the parent phase strains. The strain helps to carry out transformation by 100 %.

1.1.4 GENERAL PROBLEMS ON MAGNETIC FIELD EFFECT ON "NONMAGNETIC" SUBSTANCES

During the last 30 years there have been published over 200 studies on the effect of magnetic field with induction of 0.1–30 T and exposure time in the range of 10^{-6}–10^{6} sec on various properties of "nonmagnetic" substances (polymers, dielectric materials), semiconductors and metals [23–26]. In some cases, the magnetic field effect on some properties is more or less pronounced. For instance, in ionic crystals magnetic field affects the spin-dependent reactions between paramagnetic defects [23–27]. However, there are many examples described when the external phenomenological effects of placing the samples in the magnetic field are very similar to those presented in [23–27]. Nevertheless, the required conditions of spin-dependent reaction

occurrence are often neglected. For example, magnetic field affects the properties of metals: the microhardness values of aluminium, bronze, bismuth, etc. but during the short time of a spin reaction totally excludes the magnetic field effect on spin-dependent reactions; the influence of the properties of polymers is observed if they do not contain spin particles. Moreover, in the scientific papers it is discussed that the magnetic field has certain effects on the "aged" crystals where there are neither processes, nor reactions, therefore the magnetic field has nothing to affect. Hard to imagine that those "unpredictable" spin-dependent reactions which require meeting of a number of experimental conditions and have the chance of about a few per cent to produce the effects in chemistry [27], could occur without providing special conditions and take place in all types of the substances wherein they are reported to act as a main technique to explain the magnetic effects. Irrespectively of the fact that a lot of scientists a priori attribute a "spin-dependent" origin to the mentioned effects, they often find it difficult to identify the type of the particles with a spin. All these make perform the further studies aimed at revealing general (rather than spin-dependent) reasons why the thermodynamically weak magnetic field has an effect on the state and properties of solids. The carried out generalizing analysis on the experimental data delivered by the various scientists and addressing the physical properties of a wide range of substances regardless of their response (i.e. the physical property of a substance that has been studied in the publications) allow determining the phase of a gradual physical property change in a magnetic field and the phase of subsequent relaxation of this property after removing of the magnetic field (**Fig. 1.1**).

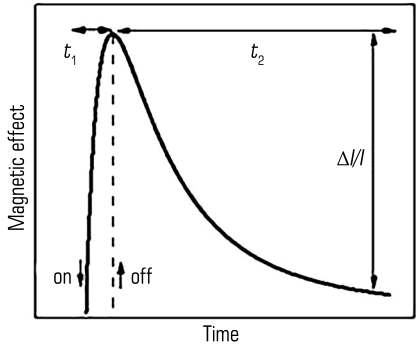

Fig. 1.1 Dependence diagram between a gradual change in the crystal physical properties within a magnetic field (with a time constant t_1) and a relaxation after the magnetic field removal (with a time constant t_2): a relative change in a physical value of $\Delta l/l$ is marked with a vertical arrow
Source: [27]

The duration of these phases (t_1 and t_2 respectively) is a universal quantitative characteristic for a number of magnetic effects. Another invariant value which can be analysed regardless

of both the measurement technique and the type of physical properties sensitive to the magnetic field is the relative value change of this property in saturation – $\Delta I/I$ (**Fig. 1.1**). By *I* we mean all the values described scientifically, whose changes under the magnetic field effect have been reported by the scientists (microhardness, dislocation pathlength, luminescence spectrum intensity, photoelectronic spectrum intensity, initial dislocation stress, electric conductivity, yield value, internal friction amplitude, etc.).

The dependence of time (t_1) on the magnetic strength in given in **Fig. 1.2**. It is obvious that regardless of the substance type and the research technique, t_1 value is subjected to a certain dependence: it reduces with the magnetic field (H) increase, i.e. magnetic induction process speeds up as the magnetic field increases. This is expected for one type of substance, but the demonstrable regularity in **Fig. 1.2** (that allows to discuss the universal dependence of $t_1(H)$ for various substances) suggests the assumption about the integral character of magnetic field physical effects on the substance properties.

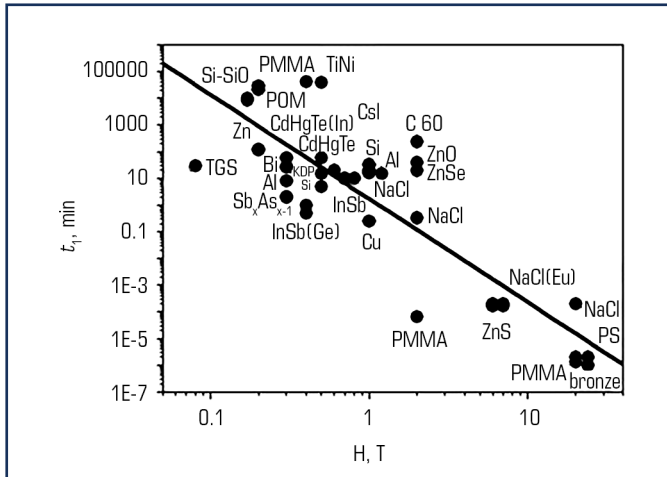

Fig. 1.2 Dependence between time t_1 and magnetic strength (H) for some substances. The approximation described in this publication is marked with a continuous line
Source: [27]

It would be natural to assume that in the magnetic field, there occur forces that affect the crystal lattice while the development of stresses changes the other properties of substances. In this case, the spread of $t_1(H)$ dependence could be explained by the difference in magnetic sensibility χ_m of solids under study. There are certain attempts to build $t_1(\chi_m H^2/2)$ dependence, where $\chi_m H^2/2$ is the magnetic field energy of the unit volume, which does not permit eliminating the spread. This indicates that the macroscopic magnetization of the substances under analysis is irrelevant for the observed effects, and the main impact on them is apparently produced

by the structure defects. In **Fig. 1.2**, the approximation of $t_1(H)$ is marked with a continuous line in double logarithmic coordinates with a linear function of $y=A+B\cdot x$, where $y=\lg t_1$, $x=\lg H$. From the approximation results, the function of $t_1=t_0/H^B$ with the parameters of $t_0=2$ min, $B=-3.9\pm0.3$ T can be drawn. Thus, the universal function is written as $t_1=t_0/H^4$. The paired measures, including the 4th-order ones, often occur in spin chemistry where the processes are governed by Δg spin contamination technique in a magnetic field [27].

Time (t_2) does not depend on the magnetic field. In thermodynamics, $t_1=t_2$ equation is applied to inverse processes. Further, if a magnetic field excites solids and transfers its energy to them, time (t_1 and t_2) are to be in a linear relation. The relaxation of an excited state should occur with the same invariable of time as the transition to excited state within the magnetic field. This is true for various processes, such as magnetization and demagnetization, chemical change in the potential with its postreduction, etc. The analysis reveals that there is no connection between t_1 and t_2 that means that the process is with the time invariable of t_2 that is often called relaxation and is in fact of a different origin. This process is represented by further transformations of the solid body defects subsystems that take place in the process with a time invariable of t_1. The attempts to obtain $t_2(H)$ dependence have been unsuccessful as well. Such dependence does not exist since the following processes that have once been initiated by the magnetic field become insensitive to the further magnetic field action and its values. The dependence between a relative change of physical properties in saturation per the time of $\Delta I/I$ is shown in **Fig. 1.3**. It turns out that the effects under study can be classified into three groups 1 (**Fig. 1.3, *a***), provided that the value of $\Delta I/I$ is built up as a magnetic energy function of a crystal lattice unit volume ($\chi_m H^2/2$). Group 1 is different from the other two groups by $\Delta I/I$ value being almost independent of the magnetic field value. Moreover, group 1 mostly includes semiconductors and metals, while in groups 2 and 3, which are highly sensitive to $\chi_m H^2/2$ value, ionic crystals and other dielectric materials prevail (**Fig. 1.3, *a***).

By this characteristic, group 2 and group 3 can be united into a single group that includes dielectric materials, which magnetic effect value depends heavily on the magnetic energy ($\chi_m H^2/2$) or (as it has been stated above) on the magnetic field. In **Fig. 1.3**, the continuous lines point to the approximation of 1, 2 and 3 types of $\Delta I/I$ dependences on ($\chi_m H^2/2$): $y=A+B\cdot x$, $y=\Delta I/I$, $x=(\chi_m H^2/2)$.

For all the three groups of substances, the magnetic effect is in a linear relation with magnetic energy $\chi_m H^2/2$. When small values of the magnetic energy of $\chi_m H^2/2$ or the weak magnetic fields, the effect is almost the same (practically identical A coefficients) and close to 5 % for each dependence of 1, 2 and 3. In large magnetic fields, B coefficient creates a large difference between 1, 2 and 3 groups.

One should mention that in spin chemistry [27], most effects are achieved by saturation in relatively low values (~0.1 T) of the magnetic fields while at values of the magnetic fields shown in **Fig. 1.3**, there is no dependence detected on the magnetic field. Thus, the established classification of the substances into groups can indicate the fact that the magnetic effects influencing semiconductors are really conditioned by spin-dependent reactions between the structure defects,

while the strong magnetic fields can activate some other magnetic field mechanisms of action in dielectric material that have not been previously discussed.

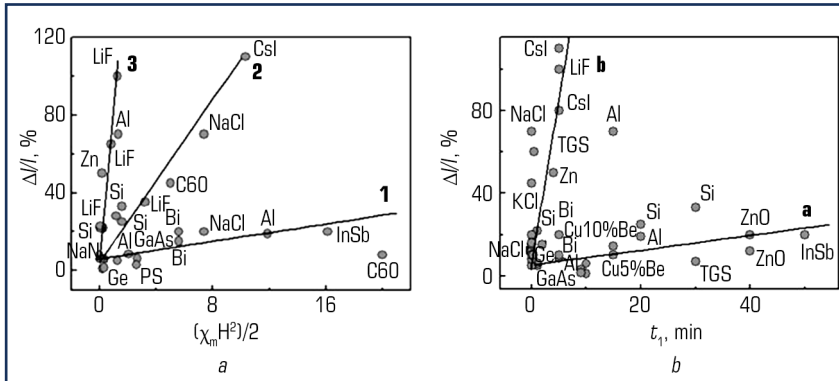

Fig. 1.3 The dependence between the relative value of property changes in solid bodies ($\Delta l/l$): *a* – the magnetic energy per unit volume ($\chi_m H^2/2$); *b* – time t_1 for some substances. The approximation described in this publication is marked with a continuous line
Source: [27]

From the above mentioned it can be obviously deduced that the magnetic effect value ($\Delta l/l$) is assumed to be related to the time (t_1) as it reflects time when waiting for the phenomenon to occur in a magnetic field and characterizes the kinetics of the change accumulation (that are induced by a magnetic field) in the crystal. **Fig. 1.3, *b*** shows $\Delta l/l(t_1)$ dependence that is also subdivided into *a* and *b* groups. Group *a* mostly includes semiconductors and metals while group *b* consists of dielectric materials. This fact emphases that there is a considerable difference in the mechanisms of the magnetic field effect on the physical properties of semiconductors and dielectric materials. **Fig. 1.3, *b*** shows the approximation of dependences $\Delta l/l(t_1)$ (marked with continuous lines) of *a* and *b* types per straight lines: $y=A+B\cdot x$, $y=\Delta l/l$, $x=t_1$ with the following parameters:

– for *a* line: $A=5.3\pm3.7$; $B=0.4\pm0.2$;

– for *b* line: $A=6.4\pm3.5$; $B=15.9\pm1.6$.

Group *b* embraces those substances, wherein the magnetic effect is in a linear relation with the time (t_1). Group *a* contains the substances with magnetic effect being independent of the time (t_1) that is expressed by a small value of *B* coefficient. The magnetic effect value ($\Delta l/l$) with short time (t_1) is almost the same (identical *A* coefficients) and close to 5 % for both *a* and *b* types of dependences.

The growing number in the publications to address the problem of a magnetic field effect on the properties of solids within the last few years allows revealing the number of general regularities for the solids:

1. Magnetic field induces the nonreversible transition to a new state after which the secondary processes occur causing sometimes the virtual crystal recovery and are perceived as "relaxation"

after being excited by a magnetic field. In fact, they are the consequences of the primary processes and are insensitive to further magnetic field effects and their values.

2. On average, for a wide range of substances (dielectric materials, metals and semiconductors), the time invariable to describe the time period of the transition into a new state decreases in its value with the magnetic field (H) increase according to the law of $t_1 = t_0/H^4$.

3. The relative change in the physical properties of solids under $\Delta l/l$ magnetic field effect in weak fields (~0.1–1 T) is the same for a wide range of substances and makes ~5 %. The influence of strong magnetic fields (3–30 T) is able to classify solids into two large groups in terms of their behaviour. Thus, the first group includes metals and semiconductors and there is $\Delta l/l$ dependence revealed on the magnetic field energy in such substance, while the second group mainly consists of dielectric materials in which $\Delta l/l$ shows strong dependence on the energy of a magnetic field per unit volume of a substance.

1.1.5 THE NATURE OF NERNST-ETTINGSHAUSEN EFFECT

Nernst-Ettingshausen effect or transverse effect is a thermomagnetic effect observed when a semiconductor with a temperature gradient is exposed to a magnetic field. This effect was discovered by Nernst and Ettingshausen in 1886, and in 1948 it was theoretically grounded by Sondheimer [28].

The nature of this effect is in the occurrence of the electric field (E) in a semiconductor and its direction is perpendicular to the temperature gradient vector (∇) and the magnetic induction vector (B), i.e. it is in the direction of the vector ($[\nabla T, B]$). If the temperature gradient and the magnetic induction are directed along X axis, then the electric field is parallel to Y axis. Therefore, there occurs the electric potential difference (u) between the points of a and b.

Both Nernst-Ettingshausen effect and Hall effect occur due to the flow divergence of charged particles caused by Lorentz force. However, there is the difference between them: Hall effect is responsible for the directed flow of particles resulted from the drift in the electric field, while in the case of Nernst-Ettingshausen effect, the same phenomenon is caused by diffusion.

The considerable difference between them is that unlike Hall constant, the sign of $q_{\perp}$ is independent of the charge carrier sign. Actually, during the drift in the electric field, the charge permutation causes the drift direction alteration, that changes the sign of Hall field.

In this case, the diffusion flow is directed from the heated end of the sample towards the cold one irrespectively to the particle charge sign. Therefore, the direction of the Lorentz force for positive and negative particles is mutually antithetic, but the direction of the electric charge flows in both cases is identical.

Longitudinal Nernst-Ettingshausen Effect.

The longitudinal Nernst-Ettingshausen effect is in the change of thermal electromotive force in metals and semiconductors under the magnetic field influence.

When the magnetic field is absent, the thermal electromotive force in electron semiconductor is defined by the difference between fast electron velocity components (drifting from the hot side) and slow electrons (drifting from the cold side) along the temperature gradient.

At the presence of the magnetic field, there is the change observed in the longitudinal components (along the temperature gradient) and transverse components (transverse to the temperature gradient) of the electron velocity, this change is dependent on the rotation angle of electron velocity in the magnetic field; the angle is defined by the time of free run of the electrons τ in metals or semiconductors.

If the time of the free run for slow electrons or electron holes (in a semiconductor) is greater than that for the fast electrons, then:

$$\upsilon_{1x}(H)/\upsilon_{1x}(0) > \upsilon_{2x}(H)/\upsilon_{2x}(0),$$

where $\upsilon_{1x}(H)$, $\upsilon_{2x}(H)$ – longitudinal components of velocities for slow electrons and fast electrons under magnetic field; $\upsilon_{1x}(0)$, $\upsilon_{2x}(0)$ – longitudinal components of velocities for slow and fast electrons when the magnetic field is absent.

The value of thermal electromotive force in a magnetic field (that is proportional to the difference of $\upsilon_{2x}(H) - \upsilon_{1x}(H)$) is higher than that when the magnetic field is absent at the difference of $\upsilon_{2x}(0) - \upsilon_{1x}(0)$; vice versa, if the time of free run for slow electrons is lower than that for the fast electrons, then the magnetic field presence decreases the thermal electromotive force.

In electron semiconductors, the thermal electromotive force increases within the magnetic field provided that there is the decrease in the time of free run τ under the increase in the electron energy (scattering at the acoustic phonons).

Within the same substances of electron semiconductors, the thermal electromotive force decreases under the magnetic field, if the time of free run τ increases with the increase in the electron energy (during the ionized impurity scattering) [29].

1.1.6 MAGNETOPLASTIC EFFECT IN DIAMAGNETIC CRYSTALS

In [30], was described the found and investigated decay of the particles from $CdCl_2$ impurity phase in monocrystalline matrix of NaCl (alkali-halide crystal) caused by magnetic field induction effect. Further, the structural changes started to appear in a few hours after the magnetic field induction treatment (the latency time) and lasted for several weeks. It has been revealed that the duration of the latency time and further structural changes are closely related to the "background" of the primary crystals. However, no physical model to explain these effects has been discussed in [30] and it is only stated that the magnetic field induction can affect the paramagnetic impurities which stabilise the quasi-equilibrium structure in primary crystals but cannot be controlled.

The direct magnetic field with the induction (0.5 T) causes the dislocation motion in NaCl and LiF crystals if no mechanical loads, thus changing the plastic properties of the sample. The established regularities of the magnetoplastic effect can be summarised as follows:

– the direction of the dislocation motion does not change during the magnetic field sign reversal (paired effect);

– the velocity of the dislocation motion is proportional to the square of the field induction and inversely proportional to the square root of paramagnetic center concentration within a crystal;

– dislocation pathlength tends to a constant value (saturation) depending upon the induction value of the magnetic field and the holding time for the crystals to spend within the magnetic field.

The paired nature of the magnetoplastic effect and its quadratic dependence on the induction value of a magnetic field imply the magnetostriction character of the phenomenon. To verify this assumption, the dedicated calibration measurement has been carried out to define the creep of NaCl samples at room temperature. At the load of ~30 kPa, the average dislocation pathlength during 5 minutes is similar to that of the magnetic field with 0.4 T induction holding (when without the load) during the same time. The revealed correlation should correspond to the magnetostriction constant of $m \sim \sigma/G \cdot B^2 \sim 4 \cdot 10^{-5}$ T^{-2}, where G is a shear modulus. However, the obtained value turns out to be several orders greater than the value of $m \leq 1.5 \cdot 10^{-9}$ T^{-2} obtained for these crystals independently.

The observed magnetoplastic effect can alternatively be explained as followings: the dislocation motion in the magnetic field occurs under the far-reaching internal stress field effects, while the magnetic field effect is narrowed to disconnecting of the dislocations from the local barriers (stoppers) through the spin-dependent electronic transitions in the magnetic field within the dislocation-impurity system.

The magnetoplastic effect, that has been evidenced by the chemical technique of double etching, necessitates the search for the similar effects in a wider range of experimental conditions, for instance: in a mode of active macrodeformation and creep, during microhardness measurement and electric dipole moment generated by the charged dislocations. These vast experiments have been carried out on the crystals of ZnS, Al, Bi, Si and InSb and C_{60} fullerite monocrystals and allow the following:

– to determine activation energy, reinforcement factor, yield point, creep rate and other magnetoplastic effect parameters as well as their dependence upon the effect produced by magnetic fields on the samples;

– to find out that the magnetic field affects these point defects of low-sensitivity which have less effective radii of interaction with the dislocations as compared to the point defects that are insensitive to the magnetic field effect;

– to reveal the magnetoplastic effect in a wide range of relative deformations ranging from ~10^{-7} to ~1 and to study this effect at different stages of macroplastic deformation;

– to establish the role of internal stresses within dislocation shears in magnetic fields when no external stresses.

The magnetic treatment of the dislocation-free crystals and the further detection of the motion in as-introduced dislocations in them reveal that within the subsystem of point defects there is the following phenomenon: the magnetically stimulated residual changes reduce the free pathlength of the dislocation under the magnetic field and increase them under conditions of mechanical load and the magnetic field absence. This difference as it has been noted earlier is conditioned in the crystals by the presence of the stoppers insensitive to the magnetic field along with magnetosensitive obstacles.

The first physical models of the magnetoplastic effect were based on the idea of the spin nature of the interaction between the dislocations and the paramagnetic point defects. Further, with the reference to this idea it was theoretically grounded, that the coeffect of the direct magnetic field and the pulsed magnetic field can cause resonance weakening of the crystals if the impulse frequency (ν) satisfies the condition of paramagnetic resonance, expressed by as given: $h\nu = g\mu_B B_0$ (h – Planck constant, g – factor of spectroscopic splitting, μ_B – Bohr magneton, B_0 – direct magnetic field induction).

Fig. 1.4 presents the dependence between the average edge dislocation pathlength and the magnetic field induction for various exposure modes. This dependence illustrates that at simultaneous exposure of NaCl:Ca (0.001 %) crystals to the magnetic fields, acting perpendicular each other, namely the direct current magnetic field and the ultrahigh-frequency magnetic field, there can be observed the maximum increase in the dislocation pathlength (L) at several discrete values of (B_0). Further, the "resonance" values of the induction correspond to $B_0 = h\nu/g\mu$, and the applied frequency of ultrahigh-frequency field is $\nu = 9.5$ GHz. Under these conditions, the resonance transitions occur between the splits from spin sublevels of electrons within the direct magnetic field and the effective factors of spectroscopic splitting $g_1 \approx 2$, $g_2 \approx 4$ and $g_3 \approx 6$, respectively.

For crystals with Eu impurities the dependence is even more complex (**Fig. 1.5**). Being obtained with the standard electron paramagnetic resonance spectrometer, the electromagnetic wave absorbance spectrum for NaCl crystals heavily doped with Eu shows the extrema.

By analysing the experimental data on the obtained magnetoplastic effects in diamagnetic crystals, there have been suggested the scheme of the probable mechanism how magnetic field effects on the evolution of metastable defect complexes. It is shown in **Fig. 1.5**.

The local minimum characterizes the profile of the elastic interaction between the constituents of the complex found in the metastable state. The solid line and the dotted lines that unite the complex constituents designate the covalent bonding in the equilibrium state and in the excited state: kT – thermally stimulated process, j – exchange integral, ΔE – exchange energy differences in S- and T-states of the complex, ν_i – frequency of transitions between absorption states that practically coincide with those in the weakening spectra, this indicates the fact that impurity ions are within the magnetosensitive complexes of defects.

According to the scheme (**Fig. 1.5**), the thermal fluctuations with the frequency (ν_1) excite the complex by covalent bonding stretching (or by changing configuration coordinates (r), such as bond angles) from the primary singlet S-state to the excited S-state. When the magnetic field does

not act, the complex, being exposed to the elastic forces from the crystal lattice, reverts to the original *S*-state due to prohibition for the complete spin that means that the complex is in dynamic equilibrium between *S*- and *S*-states.

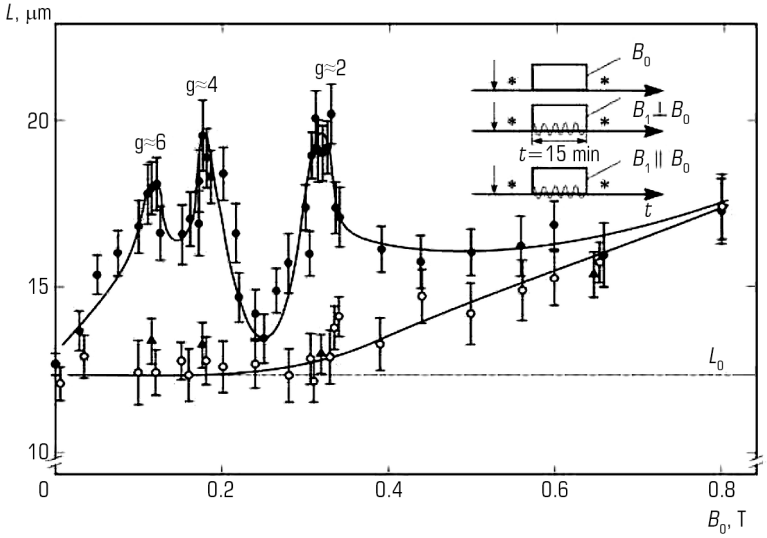

The related comments on the assignments:
○ – the absence of high-frequency current field (ν=9.5 GHz);
● – when exposed to the simultaneous action of high-frequency magnetic field and direct magnetic field in the configuration of $B_1 \perp B_0$, where B_1 – induction of the high-frequency magnetic field;
▲ – under simultaneous action of the high-frequency magnetic field and the direct magnetic field in the configuration $B_1 \parallel B_0$.

The dislocation pathlength (L_0), stipulated by the etching medium action, is shown with a shaded line for cases without external magnetic field.

The sequence of the procedures:
arrow – the inclusion of dislocations;
asterix – etching;
rectangle – exposing crystals to the magnetic field

Fig. 1.4 Dependence between the average edge dislocation pathlength (L) in NaCl:Ca crystals upon the direct magnetic field induction (B_0): exposure time of 15 min
Source: [30]

When there is a magnetic field, the prohibition is partially lifted, and the complex with $\nu_2=\mu_B B\Delta g/h$ frequency that has changed its multiplicity (Δg-mechanism of mixing states is the most probable under such conditions) evolves into a new electron *T*-state. Further, under influence

of the elastic forces from the crystal lattice there occurs reverse motion of nuclei. At that, the equilibrium R_T-state between them appears to be higher than that in the singlet *R*S-state, since the negative *J* value of exchange integrals causes the mutual repulsion of the complex constituents. Thus, with ν_3 frequency there occurs a relatively continuous triplet of *T*-state, in which the total energy of the complex constituent bonds is $\Delta E = 0.1–1$ eV, less than that in the *S*-state. The "dispersed" by this way complexes are less stable as compared to the initial ones, and the random motion of nuclei can cause either their decay with ν_4 frequency that is followed by the system escape from the local energy minimum and its further relaxation, or the restoration to the initial *S*-state with ν_5 frequency. Normally, the decay of the point defect complexes leads to the formation of weaker stoppers for the dislocations; that agrees with the experimental data on the weakening effect for the ionic crystals after they have been subjected to the magnetic fields.

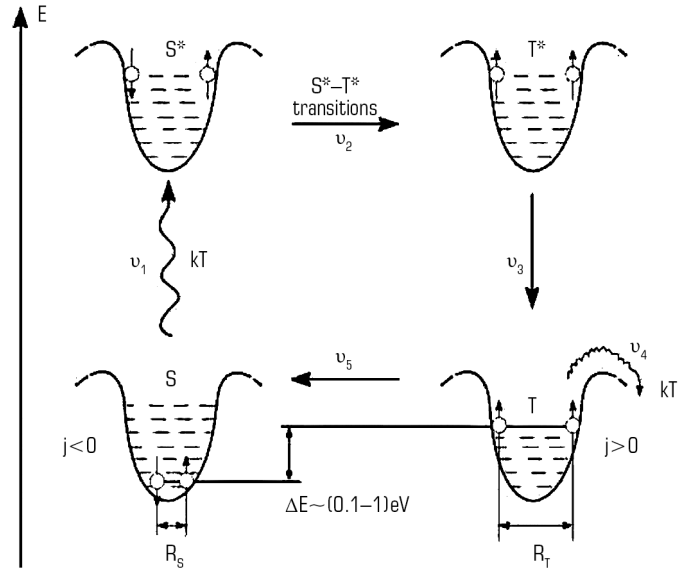

The related comments on the assignments:
S – continuous metastable singlet state of the complex;
S* – intermediate one excited by thermal fluctuations;
T* – intermediate excited triplet state, transition that is only possible in the presence of the magnetic field;
T – continuous metastable triplet state

Fig. 1.5 Schematic illustration of the process sequence in the complexes of point defects within the magnetic field: on the energy scale of *E* complex
Source: [30]

In other words it can be expressed as here: in the subsystem of the paramagnetic structural defects of the ionic crystals, spin-dependent magnetosensitive reactions are thought to considerably affect their plastic properties, while the kinetics of these reactions, according to the numerous tests, can be regulated by the weak constant fields and (what is even more efficient) by the pulsed magnetic fields.

1.2 MATERIALS AND METHODS OF THE STUDY

1.2.1 STUDY MATERIALS

In the current paper, there have been studied the samples of monocrystalline semiconductor silicon grown by Czochralski method (Cz-Si), both undoped version and doped with B, Sn, Ge, Hf, Zr, and the complexes of B-Sn and B-Mo ranging from $2 \cdot 10^{-4}$ to $8.7 \cdot 10^{-2}$ at % in initial state, after their exposure to the full heating-cooling cycle, various thermal treatment conditions and the weak direct magnetic field effect (refer to **Table 1.1**).

● **Table 1.1** Properties of the studied silicon crystals

No.	Sample characteristics (technique of preparing)	Oxygen content, atm/cm^3	Carbon content, atm/cm^3	Electric resistance at room temperature, ohm	Temperature ranges of variation lg(σ), lg(η), lg(μ) = *f*(1/*T*) from straight-line correlation							
					1		2		3		4	
					T_{start}	T_{end}	T_{end}	T_{end}	T_{start}	T_{end}	T_{start}	T_{end}
1	Float zone melting	$4\ 10^{14}$	$3\ 10^{15}$	1200	250	400	520	770	960	1005	1040	1150
2	Czochralski method, dislocation growth	10^{17}	10^{16}	25–50	260	380	770	860	960	1130	1170	1215
3	Czochralski method, dislocation-free growth	10^{17}	10^{16}	80–100	260	460	725	770	920	970	1090	1185
4	Cast polycrystalline	$2 \cdot 10^{17}$	$1.5\ 10^{18}$	0.3–3	220	320	432	555	730	918	1065	1180
5	"Raw" silicon trichlorosilane	–	–	1–20	210	350	650	750	920	960	1040	1190
6	"Raw" silicon monosilane	–	–	1–20	150	452	635	772	924	954	–	–

Source: [31]

1.2.2 METHODS OF THE STUDY

The chemical composition of the samples under analysis was determined by the spectroscopy performed at ARL-2400 testing facility.

The microstructure of the alloys was studied on the "Neophot-21" optical microscope. For revealing the general structure of semiconductor doped silicon, the samples were exposed to etching in $HF:H_2O:Cr_2O_3$ solution at the ratio of 3:3:1 with subsequent wash in the flowing water.

The temperature dependence of the thermal expansion coefficient of a semiconductor silicon was studied using the AD-80 dilatometer in the argon flow medium at the heating and cooling rate of 5 °C/min. The thermal expansion coefficient rate accuracy was 0.1 %.

The change in the solubility of doping elements (dopants) and their distribution between the structural constituents was studied by means of X-ray diffraction technique while the microhardness change was studied by means of the local X-ray spectrum analysis with MS – 46 microprobes and Camebax. XRD patterns of the alloys were recorded with DRON-3M diffractometer in k_α copper radiation. Aluminium of A999 grade and chemically pure silicon were used as reference standards. In order to determine the lattice parameters, the profiles of the diffraction extremum graphs (422) Si and (511) Si were recorded by means of the gravity center coordinate determination.

The microhardness of the modified silicon structural units was measured at PMT-3 testing facility under the load of 20 g. Each sample underwent from 36 to 76 measurements. In order to reveal the hidden regularities of silicon-based solid solution formation, the interval data imitating the distribution function [32] were used. For that purpose, the variation range of the characteristic was divided into n equal intervals and the number of cases in each interval was counted. The applied technique allowed taking into account and demonstrating silicon microhardness changes during doping.

XRD patterns of the alloys were recorded on DRON-3M diffractometer in k_α copper radiation. Chemically pure silicon was used as a reference substance.

The specific electric resistivity of doped Cz-Si was measured with 4-probe technique (the error was within of 2.5 %). The minority-carrier lifetime of charges was measured on the original testing facility for radiating heat kinetics measurement, the device built in V. Ye. Lashkaryov Institute of Semiconductor Physics of the National Academy of Sciences of Ukraine (Kyiv). The instrument accuracy was ±0.1 %.

The thermal treatment of the doped Cz-Si was performed in the laboratory in the chamber muffle kiln furnace of SNOL 2.5, 2.5/1.5. The desired temperature was maintained as accurate as ±0.5 °C by means of VRT-3 device. The temperature measurements were taken via chrome-aluminium thermocouples on R-4833 general-purpose instrument switched on according to the lattice network (the instrument accuracy of 0.05).

The magnetic treatment of the samples was carried out in the direct current magnetic field with induction of 0.066 T. The time periods of exposing for the samples were 10 and 30 days.

The measurements of the current minority-carrier lifetime after magnetic treatment were measured by the decay of the photoinduced current that occurred in the samples exposed to the GaAs light-emitting diode by means of SEMILABWT1000B device with the accuracy of ±0.1 %.

1.3 MICROSTRUCTURES OF THE SAMPLES BEFORE AND AFTER THE MAGNETIC FIELD TREATMENT

Fig. 1.6 shows the microstructures of Cz-Si samples in the initial state and after 240 and 720 hours of exposure in the direct magnetic field with the induction of 66 mT. The initial silicon microstructure is quite homogeneous with a low dislocation density (**Fig. 1.6, *a***).

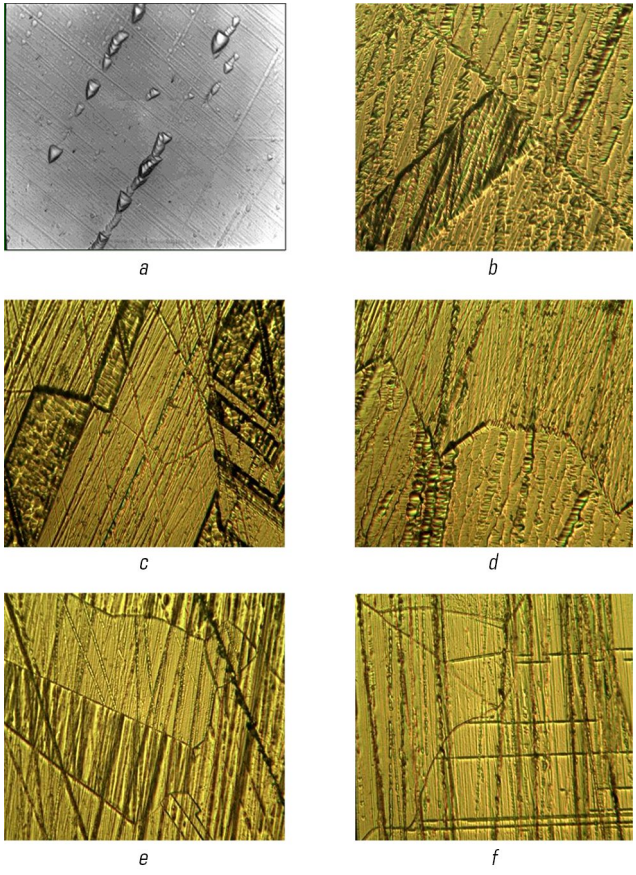

Fig. 1.6 Microstructures of Cz-Si samples: *a* – initial state, ×500; *b*, *c*, *d* – after 240 hours of exposing to direct-current magnetic field, ×400; *e*, *f* – after 720 hours of exposing to direct-current magnetic field, ×400
Source: [33–36]

240 hours of exposing to direct-current magnetic field for the monocrystalline silicon samples mean the worsening of their internal structures in terms of the significant increase in the quantity of their defects, namely the dislocation densities (**Fig. 1.6, *b–d***) and creating a great number of twins (**Fig. 1.6, *b*, *c***). However, the most interesting results revealed after the monocrystalline silicon treatment with the direct-current magnetic field are the formation of the polycrystalline silicon that is brought by the presence of a great number of grain boundaries.

The fact that the dislocation walls intersecting the grain boundaries just slightly change their directions or do not change them at all indicates that these boundaries are of the special type. The further exposing to the direct-current magnetic field has not influenced the sample microstructures except the grain sizes which become smaller (**Fig. 1.6, *e*, *f***).

The initial microstructures of the Cz-Si samples doped with aluminium (**Fig. 1.7, *a***) are characterized by rather high dislocation densities in the form of the pits after etching which form the chains. After 240 hours spent within the direct-current magnetic field (66 mT), the microstructures of the samples (**Fig. 1.7, *b–e***) show the considerable amounts of swirl-defects while the amounts of dislocations decrease to a certain degree. Etching of aluminium-doped Cz-Si samples allow to establish that 720 hours of exposing in the magnetic field result in a small quantity of single dislocations (**Fig. 1.7, *f***) and their chains in the samples but no swirl-defects have been found within such material.

The microstructures of Cz-Si samples doped with Cu are shown in **Fig. 1.8**. Initially, the samples had low densities of defects, which were mostly dislocation chains (**Fig. 1.8, *a***).

After 240 hours within the magnetic field, the sample microstructures exhibit some changes and the amount of dislocations reduces in them (**Fig. 1.8, *b*, *c***) while 720 hours of the mentioned treatment produce the effect of higher density of the chain-like dislocations in the microstructures of Si(Cu) samples as revealed after etching and comparing with the initial state (**Fig. 1.8, *e*, *f***).

In the microstructures of the Cz-Si samples doped with Zr (**Fig. 1.9**), rather high dislocation densities were found in the initial state, those dislocations were in the form of the separate pits from etching or their aggregations (**Fig. 1.9, *a***). After treating the samples with the direct-current magnetic field (B=66 mT) during the exposing time of 240 hours, the microstructures show a considerably lower number of dislocations (**Fig. 1.9, *b***). The metallographic analysis for the samples subjected to 720 hours of exposing in the magnetic field finds neither separate pits of etching nor dislocation aggregations (**Fig. 1.9, *c*, *d***), only the chains of dislocations have been revealed in these samples. In general, the microstructures have improved vs those of the samples subjected to 240 hours of exposing (this is also verified by the microhardness measurements).

In **Fig. 1.10**, we demonstrate the microstructures of Cz-Si samples doped with Hf. The microstructures of the initial samples have been characterized by rather high densities of dislocations and their regular arrangement along the certain crystallographic planes (**Fig. 1.10, *a***). Etching of the samples performed after 240 hours of the magnetic field action allows to reveal considerable quantities of swirl-defects while the dislocation densities decrease in them (**Fig. 1.10, *b–d***).

The notable changes are found in those sample microstructures which have undergone the magnetic field treatment during 720 hours. These changes can be described as follows: no swirl-defects and chains of dislocations like those revealed in the samples of 240-hour exposition; formation of large quantities of single dislocations like the pits from etching. Generally, the densities of the defects decrease in the samples of this type as compared against the samples with 240 hours of exposing.

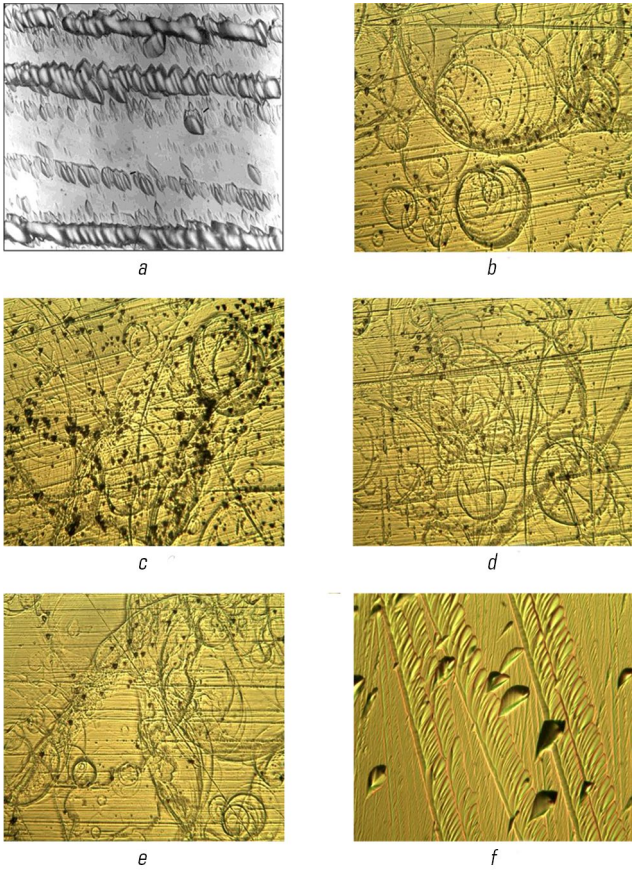

Fig. 1.7 Microstructures of Cz-Si samples doped with Al: *a* – initial state, ×500; *b*, *c*, *d*, *e* – after 240 hours of exposing to direct-current magnetic field, ×400; *f* – after 720 hours of exposing to direct-current magnetic field, ×400
Source: [33–36]

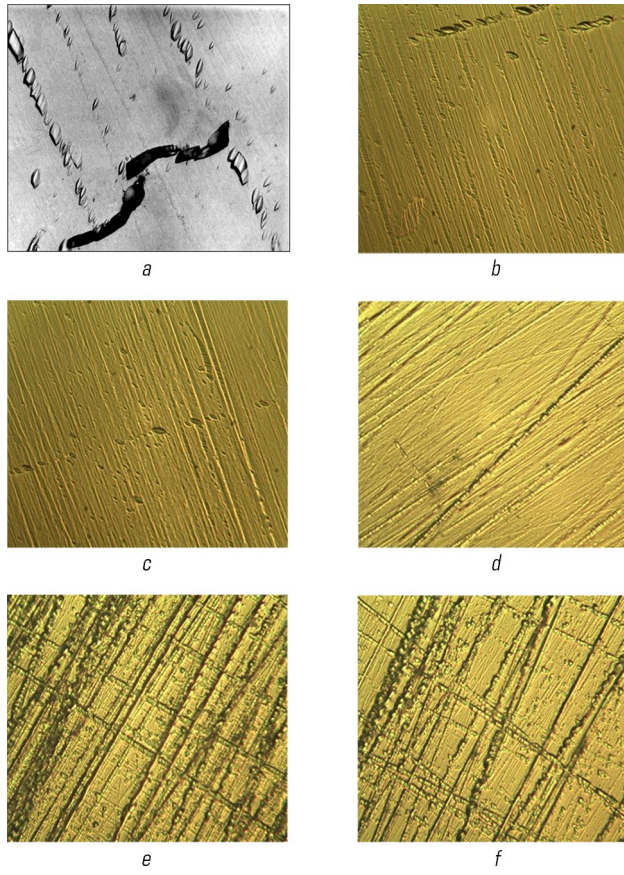

Fig. 1.8 Microstructures of Cz-Si samples doped with Cu:
a – initial state, ×500; *b*, *c* – after 240 hours of exposing to direct-current magnetic field, ×400; *d* – after 720 hours of exposing to direct-current magnetic field (sample No. 1), ×400; *e*, *f* – after 720 hours of exposing to direct-current magnetic field (sample No. 2), ×400
Source: [33–36]

In the structures of Cz-Si(Mg) samples held within the magnetic field during 240 hours (**Fig. 1.11, *b***), the considerable changes vs the initial state (**Fig. 1.11, *a***) have not been noted, however, 720 hours within the magnetic field give the rise of many single dislocations to appear in the samples, they are in the form of etching pits (**Fig. 1.11, *c*, *d***).

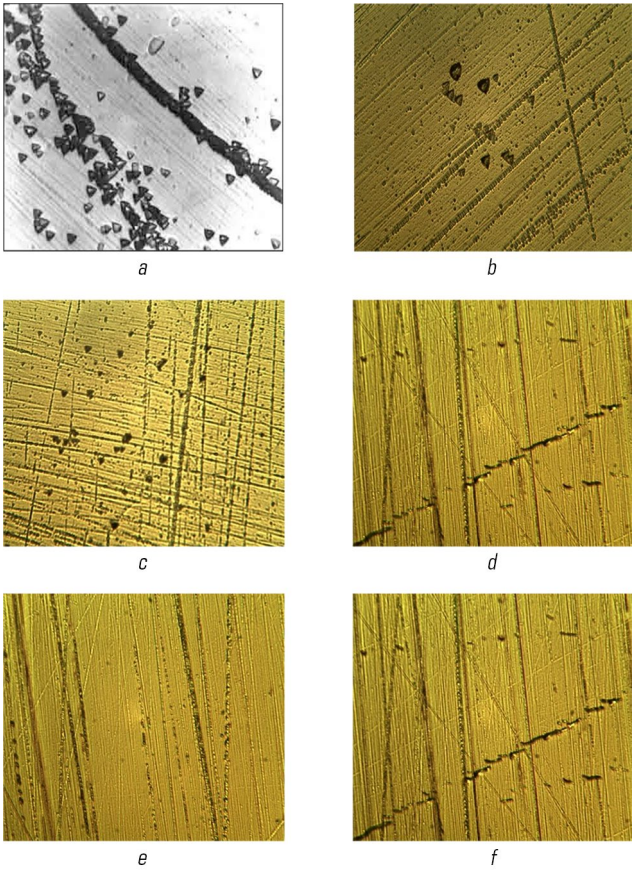

Fig. 1.9 Microstructures of Cz-Si samples doped with Zr: *a* – initial state, ×500; *b*, *c* – after 240 hours of exposing to direct-current magnetic field, ×500; *d*, *e*, *f* – after 720 hours of exposing to direct-current magnetic field, ×400
Source: [33–36]

The initial structures of Cz-Si-Fe samples (**Fig. 1.12, *a***) were with rather high densities of dislocations, arranged separately or in the form of chains. 240 hours of holding the samples within the magnetic fields enable preserving the single dislocations within the structures while the structures themselves exhibit no significant changes (**Fig. 1.12, *b, c***) in general. Further, the structures of the reported samples, which have spent 720 hours within the magnetic field, resemble their initial states, however the densities of the defects decrease (**Fig. 1.12, *d–f***).

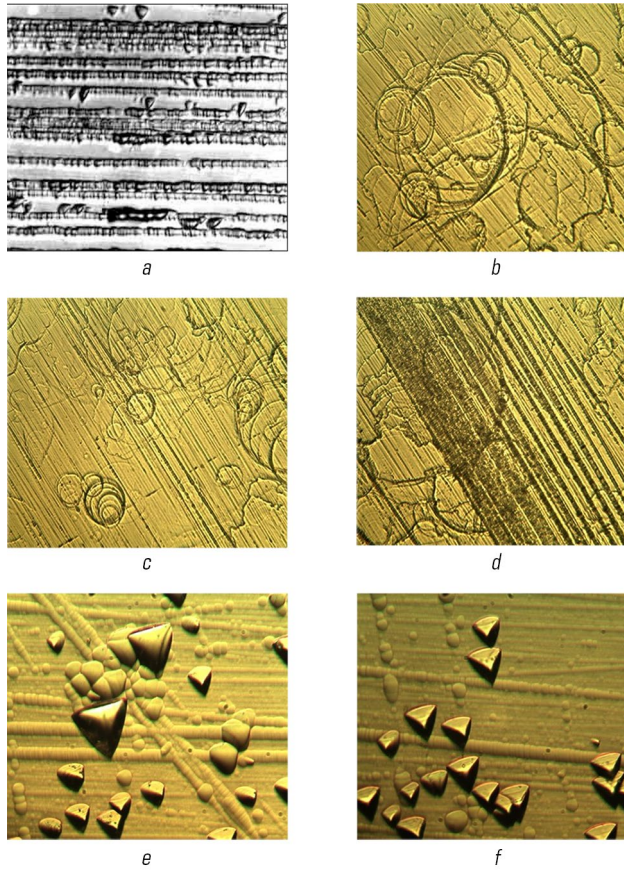

Fig. 1.10 Microstructures of Cz-Si samples doped with Hf: *a* – initial state, ×500; *b*, *c*, *d* – after 240 hours of exposing to direct-current magnetic field, ×400; *e*, *f* – after 720 hours of exposing to direct-current magnetic field, ×400
Source: [33–36]

The contemporary simulations promote the idea that magnetic field causes the spin-dependent degradation of the chemical bonds in the structural nanoclusters [37], formation of vacancy and oxygen sets (V-O, $Si_XV_YO_Z$), namely A-defects, which are able to result into the nuclei of two-dimensional defects such as dislocations [38]. The explanations on the phase transformation and the polycrystalline silicon formation in Cz-Si under the influence of the direct current magnetic field are not available in the contemporary science.

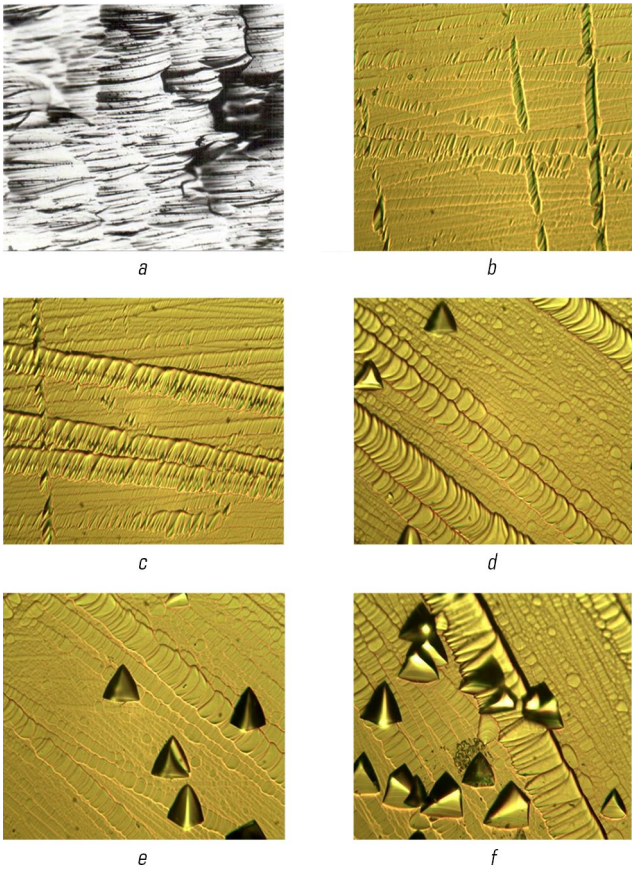

Fig. 1.11 Microstructures of Cz-Si samples doped with Mg: *a* – initial state, ×1000; *b* – after 240 hours of exposing to direct-current magnetic field, ×400; *c*, *d* – after 720 hours of exposing to direct-current magnetic field, ×400
Source: [33–36]

It can be assumed that the formation of polycrystalline silicon samples of undoped silicon is stipulated by those changes in the wave functions of the valency electron which have been produced by the direct-current magnetic field (this is confirmed by Larmor precession and the related Zeeman effect) and therefore the phenomenon is also promoted by the changes in the densities of the electron states in the space-and-time, that means the changes in the directions within which the covalent bindings occur. The rearrangement of covalent binding

orientations, in their turn, brings the changes in the crystal lattice type that means the phase transformation.

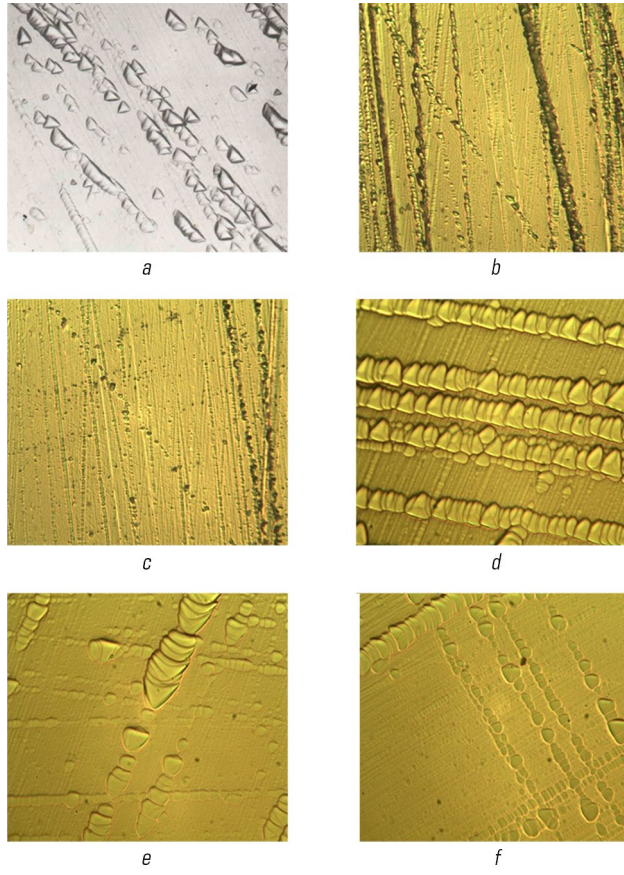

Fig. 1.12 Microstructures of Cz-Si samples doped with Fe: *a* – initial state, ×500; *b*, *c* – after 240 hours of exposing to direct-current magnetic field, ×400; *d*, *e*, *f* – after 720 hours of exposing to direct-current magnetic field, ×400
Source: [33–36]

The large number of twins formed within the structure might be assigned to the formation of silicon orthorhombic phase and silicon BCC_{III} phase with the shear pattern within the certain masses of the sample [1–4, 6]. In undoped silicon, the shear transformation of $Si_{FCC} \leftrightarrow Si_{ORTHORHOMBIC}$

occurs at the temperatures higher than 350 °C [39–43], in cases of the treatment in the magnetic field at the room temperature, this phenomenon is provoked only by the magnetic field influence. After 720 hours of exposing, there are no significant changes found in the sample structure. At this the measurements have shown the increase in the parameters of microhardness and specific electric resistance vs the samples which have been treated during 240 hours. This indicates the further proceeding of the phase transformation and the structure stabilization under the magnetic field effect.

Note that all the above-mentioned doping elements increase the critical temperatures for $Si_{FCC} \leftrightarrow Si_{ORTHORHOMBIC}$ and $Si_{ORTHORHOMBIC} \leftrightarrow Si_{BCCIII}$ (refer to **Table 1.2**). Moreover, the doping elements increase the thermodynamic stability of the closed packed phases of silicon to the magnetic field action (the magnetic field as well as the higher temperature add to the energy to the system). Furthermore, it might be assumed that the doping elements stabilise the high temperature phase of Si_{BCCIII}, thus eliminating low temperature shear-diffusion phase transformations as well as the formation of twins within the structure.

● **Table 1.2** Temperatures of phase transformation for doped silicon and the dedicated thermal expansion coefficient values

Cz-Si/doping elements	**Temperature/coefficient of thermal expansion °C/$\alpha \cdot 10^{-6} \cdot °C^{-1}$**		
	I $Si_{FCC} \leftrightarrow Si_{ORTHORHOMBIC}$	**II $Si_{ORTHORHOMBIC} \leftrightarrow Si_{BCC\ III}$**	**III $Si_{BCCIII} \leftrightarrow$ Sihcp**
Cz-Si	350/4.3	700/4.4	900/5.3
Cz-Si+Al	450/5.0	750/4.5	900/6.0
Cz-Si+Zr	500/4.5	–	850/4.7
Cz-Si+Hf	380/4.5	–	850/4.7

Source: [33–36]

Considering the influence of both the magnetic field and the doping elements on the energy of silicon interatomic bonds, it is difficult to make any assumptions since the most similar changes in the structures have been observed in the samples of Cz-Si(Al) and Cz-Si(Hf) after 240 hours and 720 hours of exposing to the magnetic field (refer to **Fig. 1.7, 1.10** respectively), despite the fact that aluminium drastically decreases the energy of silicon atom interaction while hafnium increases it greatly.

Further, the similar changes have been detected within the structures of Cz-Si(Cu) and Cz-Si(Fe) (**Fig. 1.8, 1.9**). At this, copper reduces the interaction energy of silicon atoms while iron does not bear influences on it.

In the samples of doped silicon, which has undergone magnetic field exposing during 240 hours, the increase in the defects of the inner structure can be explained via the changes in the wave functions of the electrons. Quite local is the change in the wave functions of electrons and the crystal lattice rearrangement is to provoke the breakage in covalent binding of those adjacent atoms, which wave functions will not have changed enough to meet the orientation changes of

covalent binding (the density of the electron states in the space-time). This local breakage of the atom binding is to cause the appearance of complete dislocations or partial ones together with the defects of atom packing.

The gradual decrease in both the density of the defects and the microhardness values of the structures in the samples of Si-Al, Si-Cu and Si-Zr after 720 hours spent in the magnetic field can be regarded as relevant to the structure stabilization during the time of quite long holding within the magnetic field as well as related to the decrease in the thermal capacity (enthalpy) of the system by means of annihilation of the certain portion of the structure defects. The same changes are observed in the samples during their annealing in the furnace [2].

Due to the commonly known property of aluminium to strongly decrease the energy of atom interaction in silicon, the easier shear-diffusion phase transformations within silicon occurs while hafnium influence is on the contrarily and drastically increases this energy that means slowing down the phase transformations and stabilizing the silicon structure of Si_{FCC} [31].

In order to identify the phases in the samples, which have been under the magnetic field treatment, the method of X-ray analysis have been applied. **Fig. 1.13** shows the diffractogram of Cz-Si sample in the initial state.

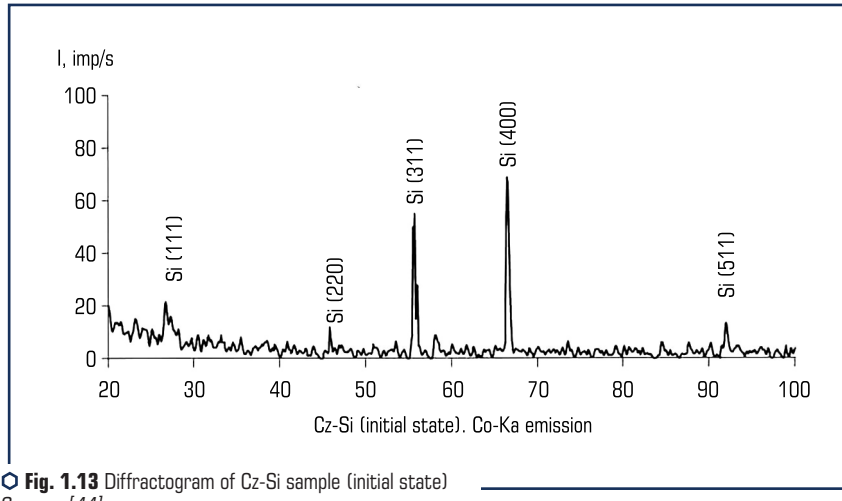

Fig. 1.13 Diffractogram of Cz-Si sample (initial state)
Source: [44]

In the initial state, Cz-Si in the diffractograms shows the reflections of FCC lattice, and line (400) possesses the maximal intensity at the scattering angles of less than 65 degrees (**Fig. 1.13**).

After treating the silicon samples with direct-current magnetic field of 0.4 T inductions, there have appeared the reflections at the scattering angles of 30–40 degrees (**Fig. 1.14**), which are interpreted as orthorhombic phase of silicon [45].

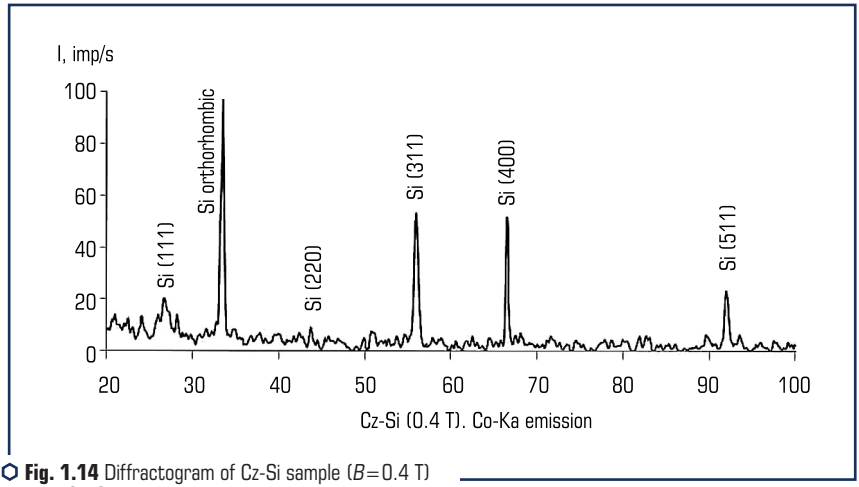

Fig. 1.14 Diffractogram of Cz-Si sample (B=0.4 T)
Source: [44]

The reflection intensityies for silicon with cubic close-packed lattice at angle of 65–70 degrees decrease after the magnetic field influence. It can be explained by phase transformation initiated in silicon, namely $Si_{FCC} \leftrightarrow Si_{ORTHORHOMBIC}$ [34] under the action of the direct current magnetic field with 0.4 T of induction.

Fig. 1.15 depicts that after treating the samples with the aggressive direct current magnetic field (B=1.2 T), there is the reduction in intensities of reflections in all the silicon phases and appears a considerable number of reflections from silicon oxide. This verifies the assumption of silicon surface activation with the direct-current magnetic field and enhancing its absorbing properties [46].

Furthermore, with the behaviour of this kind we confirm the assumption that the silicon phase structure stabilises under the action of direct magnetic field [33]. However, more detailed investigation on the line profile (511) evidences that additional phases are formed within the crystal array, and they possess the different type of the lattice.

In **Fig. 1.16**, the curves are presented to show the differential extrema (511) for the samples in the initial state and after treating with the magnetic field: B=0.4 T (*b*), 1.2 T (*c*). They have been obtained at the scattering angles of 90–92 degrees, which is the feature of silicon phase of cubic close-packed lattice [46].

The splits of the diffraction lines detect the presence of the distortions in the crystal lattices of Cz-Si samples. At this the split of the extremum (511) is to be assigned to overlapping of certain interferences of orthorhombic phase of silicon [41, 44, 45]. Further, the line splitting (511) increases with the increase in the induction of external magnetic field.

The splits of the differential extrema at the scattering angles of 90–92 degrees at higher values of external magnetic field induction evidence the presence of two phases in the silicon and

are relevant to the formation of $Si_{ORTHORHOMBIC}$ phase within this material array. The same is observed on the differential extremum split (511) at the scattering angles of 90–92 degrees after the silicon semiconductor heat treating at the temperature range of 280–450 °C, and it is assigned to the crystal lattice distortion of Si_{FCC} and formation of the certain quantity of $Si_{ORTHORHOMBIC}$ [47–48].

Eventually, the heat treatment of the silicon semiconductor gives greater splitting of the interference extremum (511) at increasing the annealing temperature from the range of 280–320 °C up to the range of 400–450 °C [48]. In the currently reported research, the significant splitting is observed at the increase of the external magnetic field induction from 0.4 T to 1.2 T. This evidences that the magnetic field and the heat treatment initiate the phase transformations of silicon.

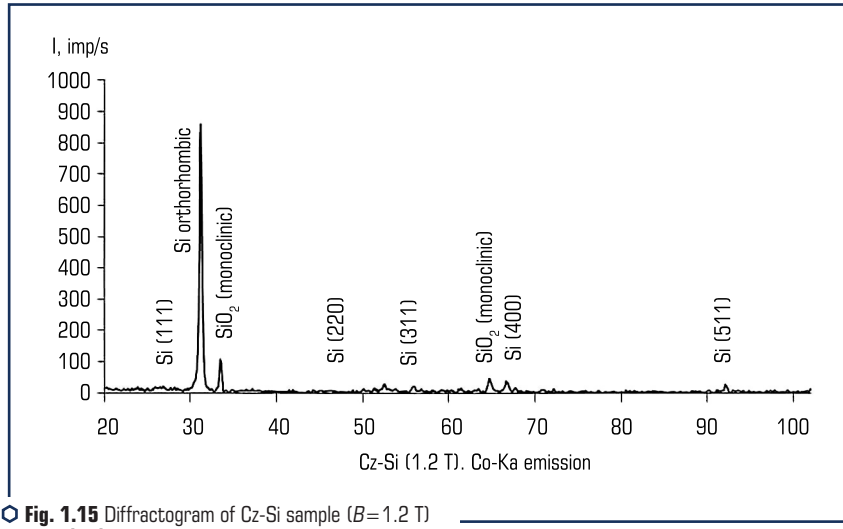

Fig. 1.15 Diffractogram of Cz-Si sample ($B = 1.2$ T)
Source: [44]

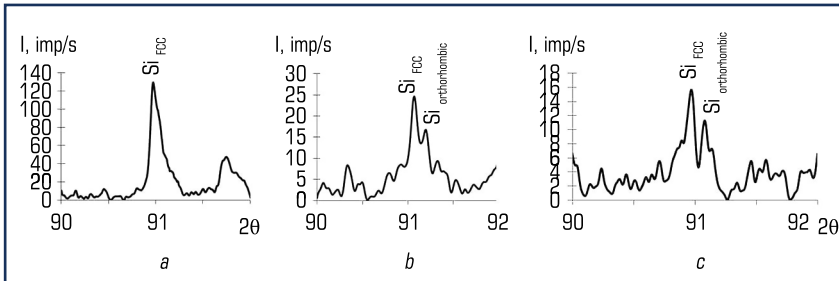

Fig. 1.16 Line profile (511) before the magnetic field action and after it: *a* – initial state; *b* – 0.4 T; *c* – 1.2 T
Source: [44]

1.4 THE SAMPLE MICROHARDNESS VALUES BEFORE AND AFTER TREATING WITH THE MAGNETIC FIELD

Magnetic field acting on Si sample has certain influence on the sample microhardness values. For the sake of the reader's swift reference we consider it is reasonable to summarise the revealed data on the microhardness change in similar patterns of representation as below.

In **Fig. 1.17**, the graphs present the microhardness values of the aluminium-doped silicon samples after 240 hours (**Fig. 1.17, *a***) and 720 hours (**Fig. 1.17, *b***) of exposing to direct-current magnetic field with the induction of 66 mT. The analysis performed for the graphs has revealed that the average microhardness of the sample matrices after 240 hours of exposition is 11000 MPa (the values vary within the range of 9000–14000 MPa), the dislocations areas demonstrate 12500 MPa (the variation range makes 11500–12500 MPa), the swirl-defect allow 10000 MPa of the value (within the range of 9000–16000 MPa).

The average microhardness per the structural units of the samples after 720 hours spent within the magnetic field becomes lower by 2500 and 950 MPa; for the matrix such change is within the range of 8500–10500 MPa while that of the dislocation areas is within the range of 9500–14000 MPa (swirl-defects have not been detected). These bring the conclusion that the ranges of the structural units' microhardness values undergo the considerable changes of decrease.

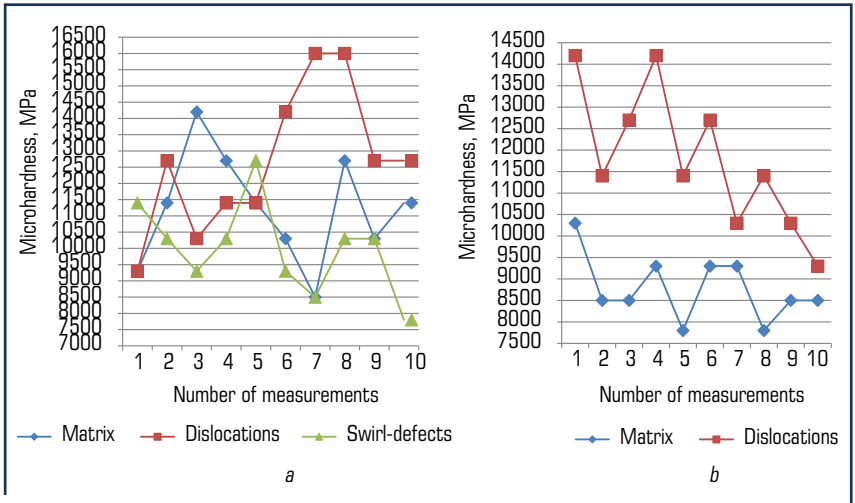

Fig. 1.17 Microhardness graphs for Cz-Si(Al) samples: *a* – after 240 hours of exposing to direct-current magnetic field; *b* – after 720 hours of exposing to direct-current magnetic field

Fig. 1.18 shows the average microhardness values per the structural units for Cz-Si(Al) samples both in the initial state and after 240- and 720-hour exposition to direct-current magnetic field.

As it can be deduced from the given bar graph, the sample microhardness values notably increase after 240 hours of exposing within the magnetic field vs the initial state of the samples. The further treating of the samples (720 hours) causes the gradual decrease in the microhardness values that is connected with the decrease in the defects of the silicon samples.

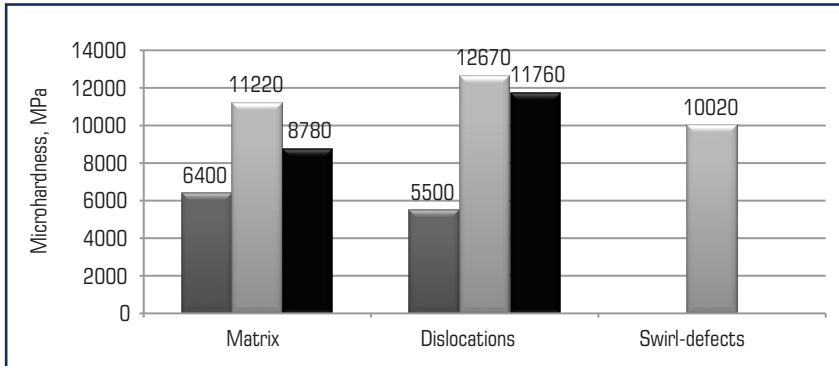

Fig. 1.18 Microhardness per the structural units for Cz-Si(Al) samples (in the initial state, after 240- and 720-hour exposition to direct-current magnetic field)

In **Fig. 1.19**, we demonstrate the microhardness graphs for Cz-Si(Hf) samples after they spent 240 and 720 hours within the magnetic field for the treatment. The average microhardness values of the structural units, which Cz-Si(Hf) samples possess after 240 hours and 720 hours of the mentioned holding, are as follows: 9000 MPa (variation range is 8500–10500 MPa) and 10400 MPa (with the variations within the range of 89500–12500 MPa) for the matrices, respectively; 12400 MPa (12500–14500 MPa) and 12700 MPa (12500–16500 MPa) for the dislocation areas.

Therefore, it follows that the increase in the holding time within the magnetic field results in higher range of the microhardness value variations that is probably connected with the increase in the defects. The microhardness parameter for swirl-defects has been revealed as much as 11000 MPa in the samples after 240-hour exposing while the etched samples of 720-hour exposing have not exhibited swirl-defects.

The microhardness average values per the structural units of Cz-Si(Hf) samples before and after the magnetic treatment are given in **Fig. 1.20**. These bar graphs show that the microhardness values gradually increase (but with slowing intensity) during further exposing to direct-current magnetic field.

In **Fig. 1.21**, we show the microhardness graphs for Cz-Si(Cu) after the action of the direct-current magnetic field. After 240 hours of magnetic field influence, the microhardness values for the matrix vary from 7100 MPa to 9500 MPa while those for the dislocation areas are within the range of 7700–11500 MPa. After 720 hours of holding, the microhardness values show

the variations from 5600 MPa to 9500 MPa for the matrix and from 6100 to 12700 MPa for the dislocation areas.

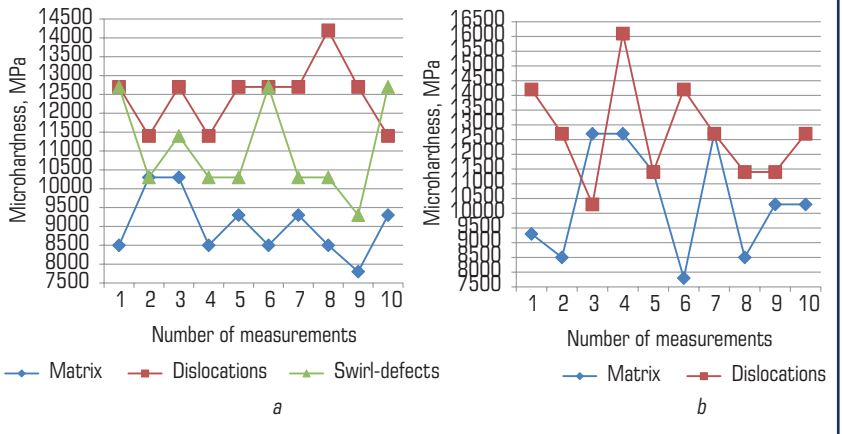

Fig. 1.19 Microhardness graphs for Cz-Si(Hf) samples: *a* – after 240 hours of exposing to direct-current magnetic field; *b* – after 720 hours of exposing to direct-current magnetic field

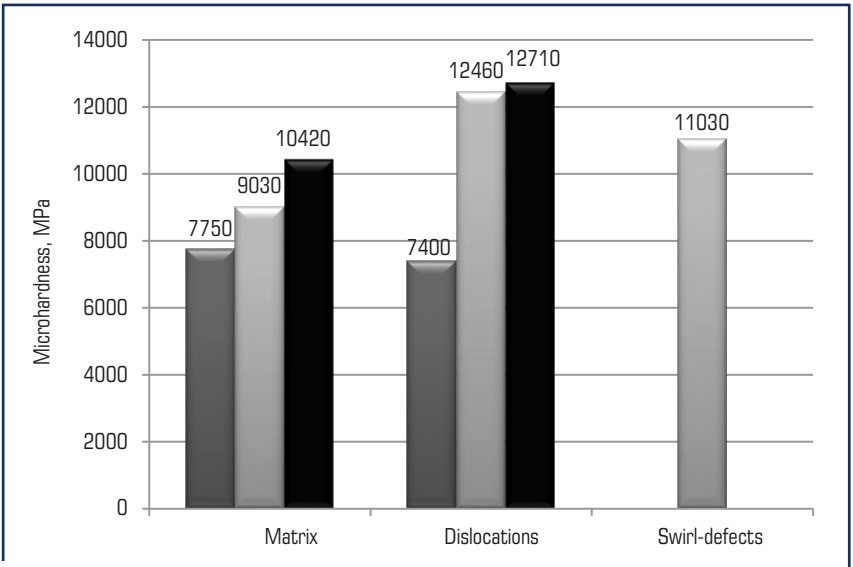

Fig. 1.20 Microhardness values per the structural units of Cz-Si(Hf) samples (in the initial state, after 240 and 720 hours of exposing to direct-current magnetic field)

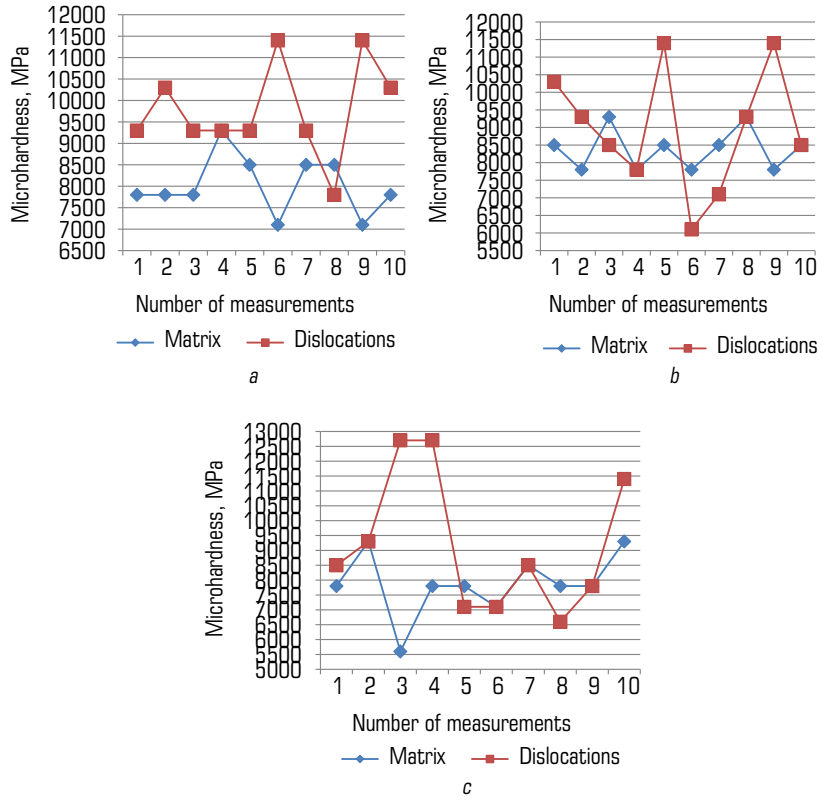

Fig. 1.21 Microhardness graphs for Cz-Si(Cu) samples: *a* – after 240 hours of exposing to direct-current magnetic field; *b*, *c* – after 720 hours of exposing to direct-current magnetic field

The average microhardness values per the structural units of Cz-Si(Cu) samples before and after the magnetic field treatment are shown in **Fig. 1.22**. Comparing with the initial state, the microhardness parameter increases by approximately 1400 MPa in the matrix and by approximately 3500 MPa for dislocations after 240 hours of the treatment. After 720 hours spent within the magnetic field, the microhardness values increase by 100 MPa more for the matrix, but the hardness of the dislocation zone decreases by 700 MPa.

In **Fig. 1.23**, the microhardness graphs of Cz-Si(Mg) samples are presented after their exposing for 240 and 720 hours within the magnetic field. The analysis of the graphs detects that after 240-hour treatment by the magnetic field, the microhardness values of the sample matrices vary from 7700 MPa up to 10300 MPa while those of the dislocation areas are within

10300–12700 MPa. After 720 hours of the magnetic field action, the microhardness values for the matrices vary 7700–11400 MPa, while for the dislocations they are 10300–12700 MPa.

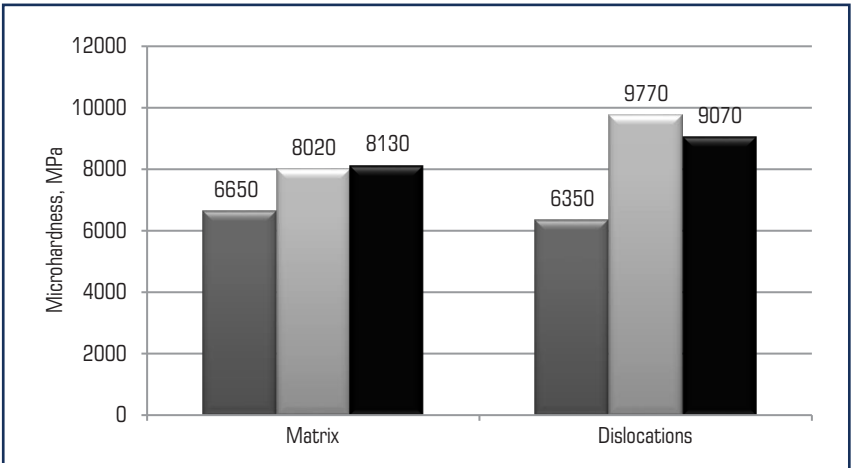

Fig. 1.22 Microhardness per the structural units of Cz-Si(Cu) samples (in the initial state, after 240- and 720-hour exposition to direct-current magnetic field)

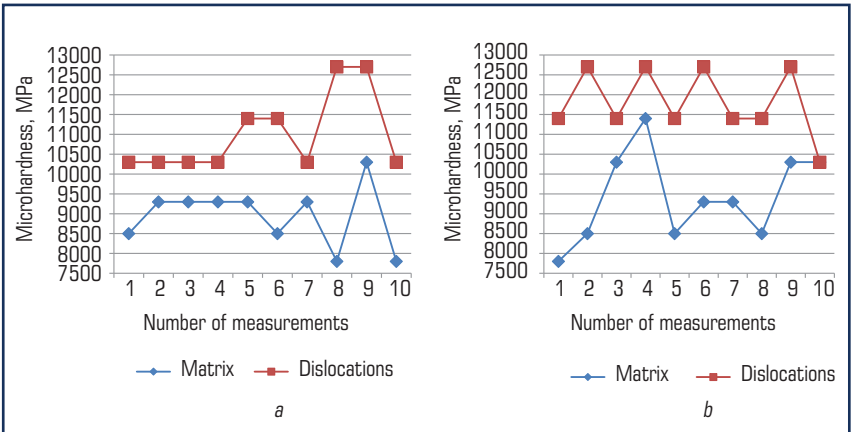

Fig. 1.23 Microhardness graphs for Cz-Si(Mg) samples: *a* – after 240 hours of exposing to direct-current magnetic field; *b* – after 720 hours of exposing to direct-current magnetic field

Fig. 1.24 presents the average values of microhardness per the structural units of Cz-Si(Mg) samples before and after treating with the direct-current magnetic field. This bar graph demonstrates that the microhardness values of the structural units increase during the time of exposing

samples within the magnetic field. After 240 hours of holding the samples, the values for the matrix microhardness increase on average as much as by 1800 MPa while in the dislocation zones such an increase is by 5000 MPa. The further treatment of the samples within the magnetic field leads to the greater microhardness values for the matrix by 500 MPa while the zone of the dislocations exhibits the increase by 800 MPa in this parameter.

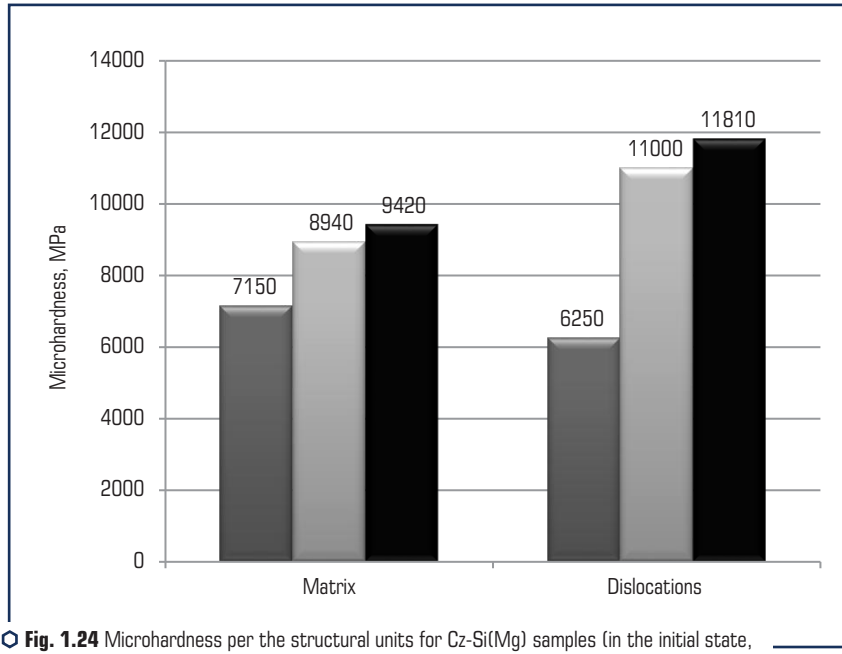

Fig. 1.24 Microhardness per the structural units for Cz-Si(Mg) samples (in the initial state, after 240 and 720 hours of exposing to direct-current magnetic field)

Fig. 1.25 reports on the microhardness graphs for Cz-Si(Fe) samples after 240 and 720 hours of their exposing within the magnetic field. The dedicated measurements on microhardness per the structural units have given the following results. After 240 hours of exposing, the matrix microhardness varies within the range of 7100–9300 MPa while the microhardness of the dislocations areas varies from 8500 to 12700 MPa. After 720 hours of exposing, the hardness for matrix is within 7100–8500 MPa and for the dislocations it is within 9300–14200 MPa.

For the average values of microhardness per the structural units of Cz-Si(Fe) samples before and after their treatment refer to **Fig. 1.26**. After 240 hours of exposing within the magnetic field, the microhardness of the matrix values grows by 1000 MPa and that of the dislocations by 4360 MPa. The further treatment causes the decrease in the matrix microhardness by 80 MPa but increase in the microhardness values of the dislocations areas by 1300 MPa.

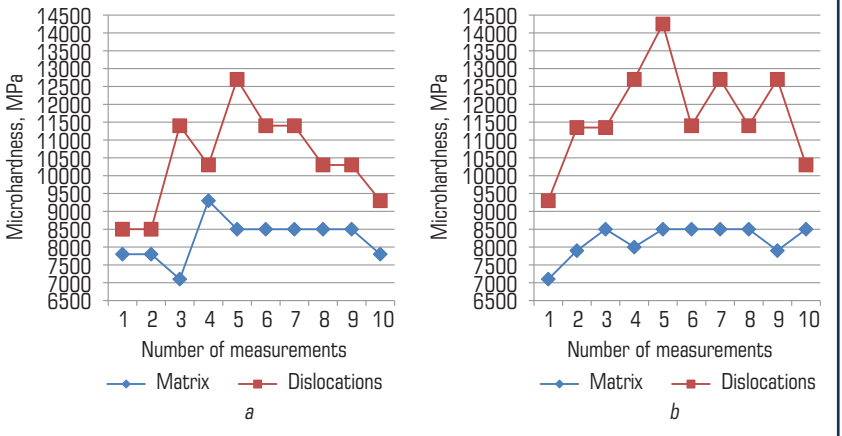

Fig. 1.25 Microhardness graphs Cz-Si(Fe) samples: *a* – after 240 hours of exposing to direct-current magnetic field; *b* – after 720 hours of exposing to direct-current magnetic field

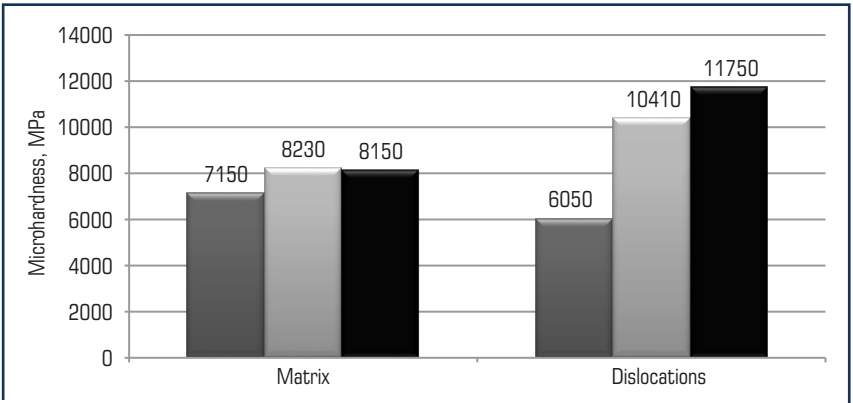

Fig. 1.26 Microhardness per the structural units of Cz-Si(Fe) samples (in the initial state, after 240 and 720 hours of exposing to direct-current magnetic field)

In **Fig. 1.27**, the microhardness average values are described graphically for the samples of Cz-Si(Zr) after 240 and 720 hours of their holding within the magnetic field. The analysis on the graphs shows that after 240 hours spent within the direct-current magnetic field, the matrix microhardness values vary within the range of 7100–14200 MPa while the dislocation areas have the range of 10300–16000 MPa for this parameter. After holding the samples during 720 hours for exposing, the matrix microhardness is 7100–11400 MPa but for the dislocation areas, it ranges within 8500–12700 MPa.

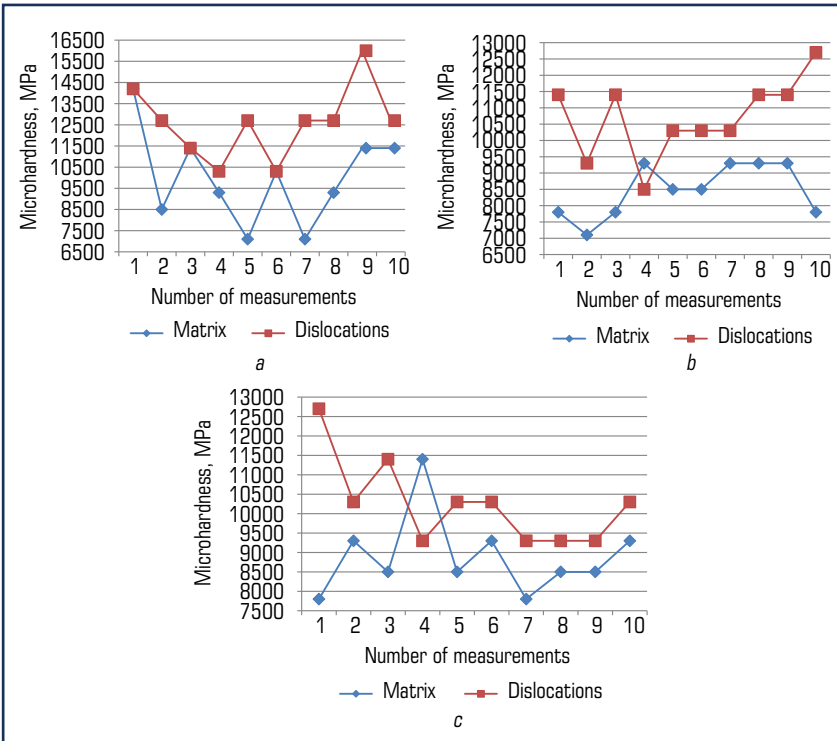

Fig. 1.27 Microhardness graphs of Cz-Si(Zr) samples: *a* – after 240 hours of exposing to direct-current magnetic field; *b*, *c* – after 720 hours of exposing to direct-current magnetic field

In **Fig. 1.28**, we report on microhardness values per the structural units of Cz-Si(Zr) samples before and after exposing to direct-current magnetic field. It is obvious from the bar graphs demonstrated that the microhardness values of the sample structural units increase after 240 hours of exposing within the magnetic field. The measurements after 720 hours of the treatment reveal that the microhardness values are smaller as compared with the values registered after 10 days of magnetic field treatment.

Fig. 1.29 represents the results of the microhardness measurements of the undoped silicon samples after their holding within the magnetic field during the period of 240 hours and 720 hours. The microhardness values of the sample matrices after 240 hours of treatment are 7400–12700 MPa, those of the dislocation areas are within the range of 7400–11400 MPa, the twin areas are 8500–16000 MPa. The microhardness values per the structural units after 720 hours of treating with the direct-current magnetic field are as follows: 8500–12700 MPa for matrix, 10300–14200 MPa for dislocation areas, 7000–14200 MPa for twins.

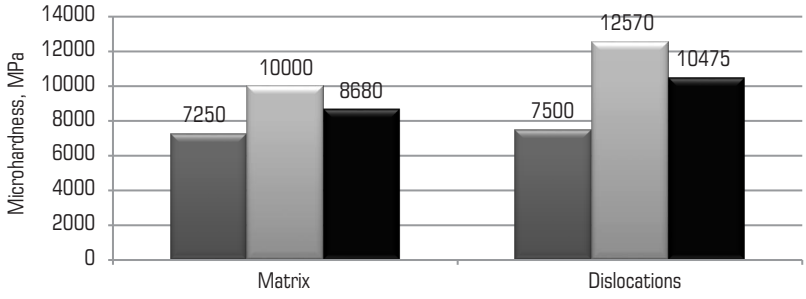

Fig. 1.28 Microhardness per the structural units of Cz-Si(Zr) samples (in the initial state, after 240 hours and 720 hours of exposing to direct-current magnetic field)

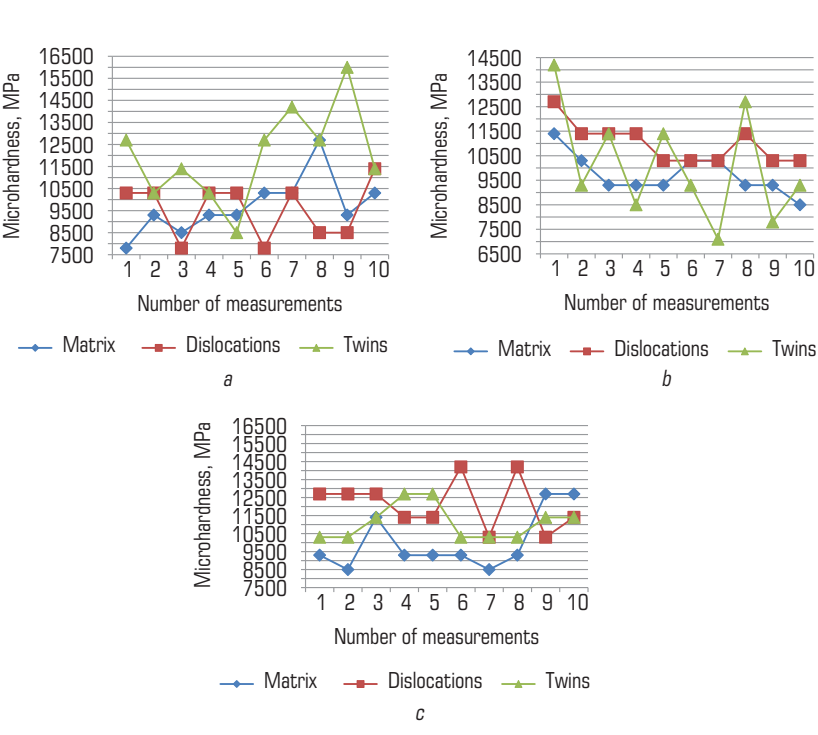

Fig. 1.29 Microhardness graphs of Cz-Si samples: *a* – after 240 hours of exposing to direct-current magnetic field; *b*, *c* – after 720 hours of exposing to direct-current magnetic field

The microhardness values per the structural units of undoped silicon samples before and after their treating with the magnetic field are reported in **Fig. 1.30**.

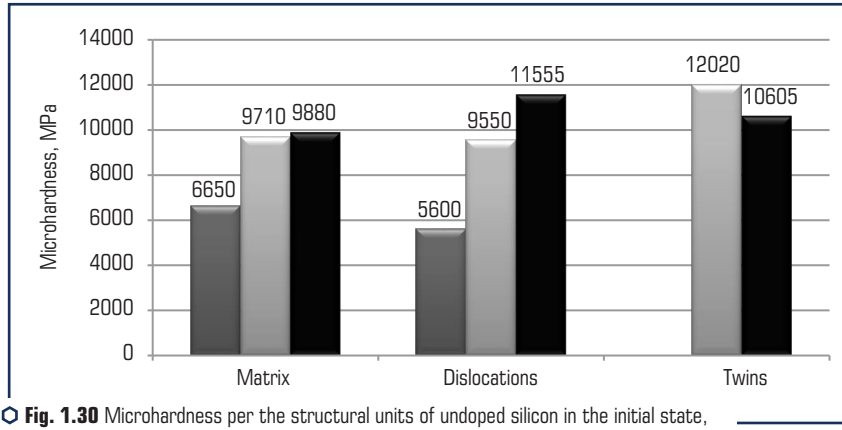

Fig. 1.30 Microhardness per the structural units of undoped silicon in the initial state, after 240 and 720 hours of exposing to direct-current magnetic field

After 240 hours spent within the magnetic field, the matrix microhardness values grow stronger by 3000 MPa, the dislocation area microhardness shows the increase by 3900 MPa, a large quantity of twins appears and their average microhardness is 12000 MPa. After 720 hours of holding within the magnetic field, the microhardness values go up for the certain structural units as given: within matrix – by 200 MPa, within the dislocation zones – by 2000 MPa; however the microhardness values of twins decrease by 1500 MPa.

1.5 THE PHYSICAL PARAMETERS OF THE SAMPLES BEFORE AND AFTER TREATING WITH THE MAGNETIC FIELD

Table 1.3 reports on the values of the physical parameters and the mechanical properties of the samples of both undoped and doped silicon before and after treating with the magnetic field induction of 66 mT.

In the initial state, the highest values of the specific electric resistance are possessed by Si-Zr sample, the lowest ones are the characteristics of the undoped silicon. The longest lifetime for the current minority-carriers is observed with the samples of the undoped silicon.

The date presented in the table evidence that there is a significant decrease observed in the values of the specific electric resistance and the life time for the current minority-carriers after the treating the samples of doped silicon within direct-current magnetic field. For the samples of undoped silicon, the decrease in the life time for the current minority-carriers is as great as several orders.

● **Table 1.3** Physical parameters and mechanical properties of the doped silicon samples before and after exposing to direct-current magnetic field

Sample	Properties	Initial State	240 hours of exposing	720 hours of exposing
Cz-Si	ρ, Ohm·cm	80–100	46–49	83–92
	t, μs	574	0.65	0.63
	Conduction type	P	p	P
	Hμ, MPa	6500	9500	9600
Cz-Si-Al	ρ, Ohm·cm	200–210	55–65	60–65
	τ, μs	12.1–12.5	0.40	0.32
	Conduction type	P	p	P
	Hμ, MPa	6800	10750	10320
Cz-Si-Hf	ρ, Ohm·cm	180–192	12.8–14.3	13.5–14.0
	τ, μs	148	23.08	28.11
	Conduction type	P	p	P
	Hμ, MPa	7750	10500	10900
Cz-Si-Cu	ρ, Ohm·cm	170–190	44.8–46.2	43.7–50.0
	τ, μs	134–138	16.32	14.55
	Conduction type	P	p	P
	Hμ, MPa	6900	10450	10700
Cz-Si-Zr	ρ, Ohm·cm	308–324	13.0–23.5	22.5–25.6
	τ, μs	228	93.3	69.57
	Conduction type	N	n	N
	Hμ, MPa	7900	11200	10300

Source: [33]

All the samples exhibit the drastic drop of the electric resistance after 240 hours of exposing to direct-current magnetic field, however some increase is observed in the values of this parameter with the further treatment by holding the samples in the magnetic field (Si-Cu behaved as an exception to this regularity). The sharp drops of the life times of the current minority-carriers are registered with all the samples after 240 hours of holding within the magnetic field, and they are followed by the further decrease if the holding time of 720 hours (however Si-Hf has been an exception).

In **Fig. 1.31**, we show the dependences between the life times of the current minority-carriers and the average microhardness for the undoped and the doped silicon samples before and after treating the samples with the direct-current magnetic field.

For the samples in their initial state, the dependence is discernible between the microhardness value and the life time of the current minority-carriers. After treating them with the magnetic field,

this dependence considerably weakens and the notable irregularities in it are found if we study the Si samples doped with Zr, Hf (**Fig. 1.31, *b, c***) and Mg (**Fig. 1.31, *c***).

Shortening the life time for the current minority-carriers can be explained as the relevance with that oxygen which the silicon surficial layers contain. As the publication reports [34], during the time when silicon is treated within the magnetic field, the oxygen content increases drastically in its surficial layers, the same is true for the ions of the alkaline metal (K^+, Na^+), hydroxyl groups and other radicals. This is related to the surface activation and enhancing its absorption ability under the influence of weak magnetic field.

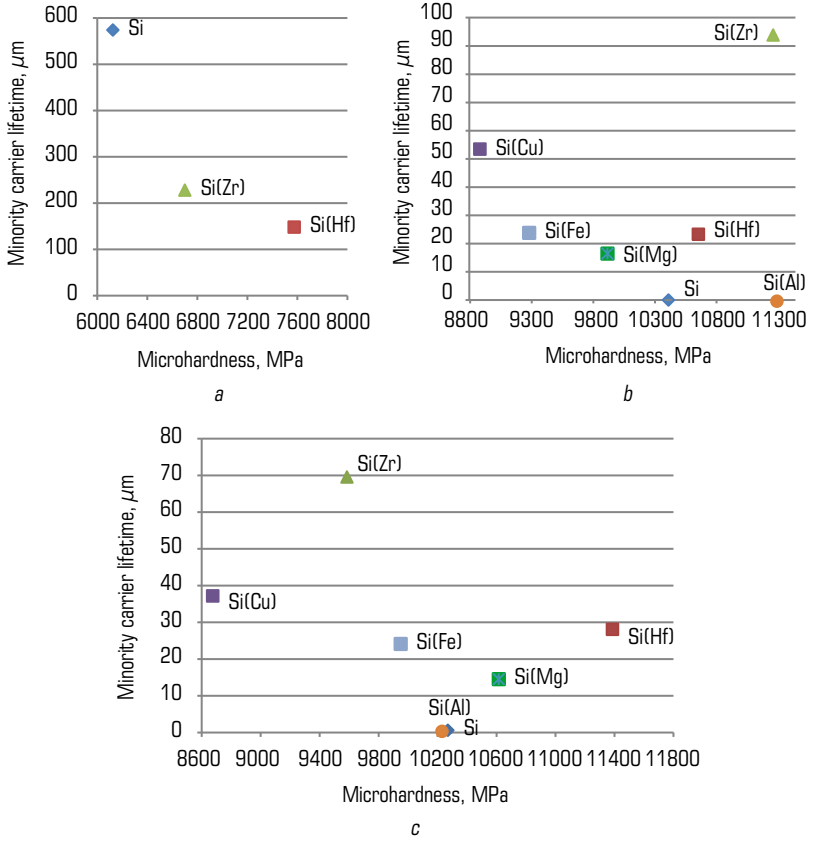

Fig. 1.31 Dependence between the time span of the current minority-carriers and the average microhardness of the samples: *a* – initial state; *b* – after 240 hours of exposing to direct-current magnetic field; *c* – after 240 hours of exposing to direct-current magnetic field

Apart from the oxygen in the principle state or the triplet state, the radical groups absorbed on the silicon surface also possess the ability of capturing the current carriers [33] and drastically decrease their lives in the free state.

Doping silicon with the elements of a greater affinity for oxygen (Zr, Hf, Al) permits the decrease in the influence of oxygen on the charge carrier life time by its binding. This is an assumable explanation for the reason why the samples doped with the mentioned elements have quite high values for the auxiliary charge carrier life time if the microhardness values are also high. The exception to this regularity is Si(Al).

CONCLUSIONS

1. The microstructure of the initial Cz-Si sample which is formed under the influence by the treatment within the magnetic field has been not studied before the research conducted for the current publication. The research reveals as follows:

– during 240 hours of exposing to the magnetic field, there is the significant increase in the number of the internal structure defects and the density of the dislocations as well as the formation of twins;

– during 720 hours of treating within the magnetic field, the polycrystalline silicon is formed with a large quantity of grain boundaries.

2. This research is the first time when it has been addressed to the problem of the magnetic field influences on the microstructure of Cz-Si doped with the elements which influence differently the energy of interaction between the silicon atoms within the crystal lattice, namely – Al, Mg, Cu, Fe, Zr, Hf.

With this publication, we show what influence produces the treatment within the magnetic field on Cz-Si doped with those elements which are able to decrease the interaction energy of silicon atoms (Al, Mg, Cu, Fe).

The data revealed can be summarized as follows:

– there is an increase in the quantity of the sample structural defects at exposing during 240 hours but their notable decrease is observed during 720 hours;

– Cz-Si doped with Zr and Hf, which increase the energy of interaction between the silicon atoms within the lattice, goes down significantly in the quantity of structural defects starting from at the point of 240 hours spent within the magnetic field.

3. By means of X-ray analysis conducted for the samples, which have been subjected to the magnetic field, it is registered that there are splits in the diffraction lines as well as the appearance of the new peaks at the scattering angles of 90–92 degrees. These phenomena are caused by the distortions of Si_{FCC} crystal lattice and forming $Si_{ORTHORHOMBIC}$ along with it. This evidences about the phase transformations in the samples of the semiconductive silicon when the magnetic treatment at the room temperature.

4. The study performed to address the problem of magnetic field influence on the microhardness of the doped Cz-Si has revealed as follows:

– the microhardness of Cz-Si doped with Al, Mg, Cu, Fe grows by 1.8–2.0 times at exposing both during 240 hours and 720 hours;

– the microhardness of Cz-Si doped with Zr, Hf grows by 1.5–1.8 times after exposing to the magnetic field during 240 hours while such values are higher by 1.2–1.5 times after 720 hours of exposition.

5. In this publication, the problem of the magnetic field treatment is first studied in terms of its influence on the physical properties of the doped Cz-Si, namely, its specific electric resistance (ρ, Ohm·cm), life time (τ, μs). It has been revealed as follows:

– 240 hours spent within the magnetic field decrease the specific electric resistance (ρ, Ohm·cm) of Cz-Si by 1.7–2.0 times while 720 hours of exposing decrease this parameter by 1.08;

– specific electric resistance (ρ, Ohm·cm) of Cz-Si Al, Cu decreases by 3.4 times at exposing within the magnetic field during the time period from 240 to 720 hours;

– for Cz-Si doped with Zr we observe the decrease in specific electric resistance values (ρ, Ohm·cm) by 18 times after 240 hours of the mentioned exposing and by 13.5 times at 720 hours of exposition;

– for Cz-Si doped with Hf, the specific electric resistance decreases by 13.5 times after 240 and 720 hours of exposing;

– the life time for minority-carriers of the charge (τ, μs) decreases 900 times within Cz-Si under conditions of both 240 and 720 hours of the magnetic field treatment;

– for Cz-Si doped with aluminium, the life time for minority-carriers of the charge decreases by 30 times when 240 hours of treatment while the decrease in 38 times is detected after 720 hours of exposing;

– for Cz-Si doped with copper, the life time for its minority-carriers of the charge decreases by 8–9 times both under 240 hours and 720 hours within the magnetic field;

– for Cz-Si doped with hafnium, the life time for its minority-carriers of the charge (τ, μs) decreases by 6 times at 240 hours and by 5 times at 720 hours of exposing;

– doping with zirconium enables sustaining the longest life times for its minority-carriers of the charge (τ, μs) vs those of the initial state: the life time for its minority-carriers of the charge experiences the shortening just by 2.4–3.2 after exposing within the magnetic field during 240 and 720 hours and they correspond to the values of 93.3 μs and 69.57 μs, respectively, compared against 0.63–0.65 of Cz-Si.

6. In this publication, we report on the development of the new complex production technology for silicon semiconductor. The technology includes the stages of silicon doping with the transition metals and rare earth metals, heat treatment at the temperatures of phase transformations and treating within the magnetic field at room temperature. These stages provide the enhanced set of the mechanical and the physical properties for Cz-Si products intended for devices.

REFERENCES

1. Glazov, V. M., Timoshina, G. G., Mikhailova, M. S. (1996). Printcipy legirovaniia kremniia dlia povysheniia ego termostabilnosti. Doklady Akademii Nauk, 347 (3), 352–355.
2. Taran, Yu. N., Glazov, V. M., Regel, A. R., Kutsova, V. Z., Koltsov, V. B., Timoshina, G. G. et al. (1991). Strukturnye prevrashcheniia pri nagreve monokristallov kremniia Fizika i tekhnika poluprovodnikov, 4 (25), 588–595.
3. Kol'tsov, V. B., Zubkov, A. M., Timoshina, M. I. (2002). Metodika issledovaniy elektrofizicheskikh svoystv monokristallov kremniya v shirokom intervale temperatur. Fizika poluprovodnikov i polumetallov. Saint-Petersburg.
4. Kozhitov, L. V., Botavin, V. V., Shepel, P. N., Timoshina, G. G., Timoshina, M. I. (2002). Issledovanie kinetiki raspada kremniia, legirovannogo perekhodnymi i redkozemelnymi elementami. Kremniy-2002. Novosibirsk, 129.
5. Novokhatskiy, I. A., Kisun'ko, V. Z., Ladyanov, V. I. (1985). Osobennosti proiavlenii razlichnykh tipov strukturnykh prevrashchenii v metallicheskikh rasplavakh. Izvestiya vuzov. Chernaya metallurgiya, 5, 1–9.
6. Kutsova, V. Z., Nosko, O. A., Timoshina, M. I. (2006). Alloying effect on structure and properties of semiconductor silicon. Proceeding of the International Conference Silicon 2006, 450–459.
7. Tonkov, E. Yu. (1988). Fazovye prevrashcheniia soedinenii pri vysokom davlenii. Vol. 1, 2. Moscow: Metallurgiya, 463, 356.
8. Kutsova, V. Z., Nosko, O. A., Timoshina, M. I. (2007). Vliianie legiruiushchikh elementov na strukturu, fazovyi sostav i svoistva poluprovodnikovogo kremniia. Kremniy-2007. Moscow: Gosudarstvennyy tekhnologicheskiy universitet "Moskovskiy institut stali i splavov", 109.
9. Glazov, V. M., Zemskov, B. S. (1967). Fiziko-khimicheskie osnovy legirovaniia poluprovodnikov. Moscow: Nauka, 372.
10. Klevan, O. S., Engh, T. A. (1995). Dissolved impurities and inclusions in FeSi and Si, development of a filter sampler. INFACON 7. Trondheim, 441–451.
11. Prikhodko, E. V. (1983). Metallokhimiia kompleksnogo legirovaniia. Moscow: Metallurgiya, 184.
12. Nesterenko, A. M., Uzlov, K. I., Kutsova, V. Z., Nyshchenko, A. N. (1988). Vliianie skorosti okhlazhdeniia na obrazovanie tverdykh rastvorov v sisteme Al-Si. Izvestiya AN SSSR, Metally, 2, 192.
13. Savitskiy, E. M., Burkhanov, S. S. (1967). Metallovedenie tugoplavkikh metallov i splavov. Moscow: Nauka, 324.
14. Liubov, B. Ia. (1969). Kineticheskaia teoriia fazovykh prevrashchenii. Moscow: Metallurgiia, 264.
15. Taran, Yu. N., Kutsova, V. Z., Uzlov, K. I., Falkevich, E. S. (1992). Shearing phase transformations in semiconductors. Proceeding of the International Conference 'Silicon 92', 88–95.
16. Milvidskiy, M. G., Osvenskiy, V. B. (1984). Strukturnye defekty v monokristallakh poluprovodnikov. Moscow: Metallurgiya, 256.

17. Glazov, V. M., Koltsov, V. B., Kutsova, V. Z., Taran, Yu. N., Timoshina, G. G., Uzlov, K. I., Falkevich, E. S. (1990). Issledovanie elektro-fizicheskikh svoystv kremniya v shirokom intervale temperatur. Elektronnaya tekhnika, 11.
18. Glazov, V. M., Kurbatov, V. A., Koltsov, V. B. (1985). Issledovanie effekta Kholla antimonidov Ga i In v tverdom i zhidkom sostoyanii. Fizika i tekhnika poluprovodnikov, 19 (4), 662–667.
19. Kopaev, Iu. V., Meniailenko, V. V., Molotkov, S. N. (1985). Neravnovesnye fazovye perekhody v kovalentnykh poluprovodnikakh pod vozdeistviem lazernogo izlucheniia. Fizika tverdogo tela, 27 (11), 3288–3294.
20. Landau, L. D., Lifshits, E. M. (1964). Statisticheskaia fizika. Moscow: Nauka, 568.
21. Tairov, Yu. M., Tsvetkov, V. F. (1980). Rost kristallov i politipizm karbida kremniya. Rost kristallov, 13, 104–111.
22. Taran, Yu. N., Kutsova, V. Z., Chervonyy, I. F., Shvets, E. Ya., Falkevich, E. S. (2004). Poluprovodnikovyy kremniy: teoriya i tekhnologiya proizvodstva. Zaporozhe: Zaporozhskaya gosudarstvennaya inzhenernaya akademiya, 344.
23. Alshits, V. I., Darinskaya, E. V., Koldaeva, M. V., Petrzhik, E. A.; Hirth, J. P. (Ed.) (2008). Magnetoplastic Effect in Nonmagnetic Crystals. Dislocations in solids. Amsterdam: Elsevier, 14 (86), 333–437. https://doi.org/10.1016/s1572-4859(07)00006-x
24. Alshits, V. I., Darinskaya, E. V., Koldaeva, M. V., Petrzhik, E. A. (2003). Magnetoplastic effect: Basic properties and physical mechanisms. Crystallography Reports, 48 (5), 768–795. https://doi.org/10.1134/1.1612598
25. Golovin, Yu. I. (2004). Magnitoplastichnost tverdykh tel (Obzor). Fizika Tverdogo Tela, 46, 769.
26. Morgunov, R. B. (2004). Spinovaia mikromekhanika v fizike plastichnosti. Uspekhi fizicheskikh nauk, 174, 131–153.
27. Buchachenko, A. L. (2013). Mass-Independent Isotope Effects. The Journal of Physical Chemistry B, 117 (8), 2231–2238. https://doi.org/10.1021/jp308727w
28. Zinenko, V. N., Sorokin, B. P., Turchin, P. P. (1983). Osnovy fiziki tverdogo tela. Moscow: Vysshaia shkola, 330.
29. Milnes, A. G., Feuch, D. L. (1972). Heterojunctions and Metall-Semiconductor Junctions. New York; London: Academic Press, 418. https://doi.org/10.1016/b978-0-12-498050-1.x5001-6
30. Zhitinskaya, M. K., Nemov, S. A., Svechnikova, T. E. (1997). Vliyanie neodnorodnostey kristallov Bi_2Te_3 na poperechnyy effekt Nernsta – Ettingsgauzena. Fizika i tekhnika poluprovodnikov, 31 (4), 441–443.
31. Chervonyi, I. F., Kutsova, V. Z., Pozhuiev, V. I., Shvets, Ye. Ya., Nosko, O. A., Yehorov, S. H., Voliar, R. M. (2009). Napivprovidnikovyi kremnii: teoriia i tekhnolohiia vyrobnytstva. Zaporizhzhia, 350.
32. Vapnik, V. N. (Ed.) (1984). Algoritmy i programma vosstanovleniya zavisimostey. Moscow: Nauka, 816.
33. Kutsova, V. Z., Nosko, O. A., Tutyk, V. A., Sulay, A. M. (2015). Struktura, mekhanichni ta elektrofizychni vlastyvosti monokrystalichnoho kremniiu pid diieiu postiinoho mahnitnoho polia. Metallurgicheskaya i gornorudnaya promyshlennost, 1, 73–79.

34. Kutsova, V. Z., Nosko, O. A., Sulay, A. M. (2014). Vliianie legirovaniia i termicheskoi obrabotki na strukturu i svoistva poluprovodnikovogo kremniia. Metallurgicheskaya i gornorudnaya promyshlennost, 6, 65–72.
35. Kutsova, V. Z., Nosko, O. A., Sulay, A. M. (2015). The structure, mechanical and electrophysical properties of monocrystalline silicon under influence of constant magnetic field. Ukrainian journal of mechanical engineering and materials science, 1 (1), 91–98.
36. Kutsova, V. Z., Nosko, O. A., Sulai, A. M. (2017). The influence of constant magnetic field on the structure and properties of monocrystalline silicon. Metaloznavstvo ta termichna obrobka metaliv, 2, 32–40.
37. Bonch-Bruevich, V. P., Kalashnikov, S. G. (1990). Fizika poluprovodnikov. Moscow: Nauka, 685.
38. Moss, T. S., Burrell, G. J., Ellis, B. (1973). Semiconductor opto-electronics. Butterworth-Heinemann, 441. https://doi.org/10.1016/c2013-0-04197-7
39. Kutsova, V. Z., Uzlov, K. Y., Khronenko, V. M. (1999). Temperaturnaya zavisimost' otnositel'nogo udlineniya sverkhchistogo kremniya. Metallurgicheskaya i gornorudnaya promyshlennost, 4, 72–74.
40. Taran, Iu. N., Kutcova, V. Z., Kovalchuk, M. G., Uzlov, K. I. (1988). Neodnorodnost beta-tverdogo rastvora v siluminakh. Metallovedenie i termicheskaia obrabotka metallov, 9, 33–37
41. Taran, Yu. N., Kutsova, V. Z. (2002). Fazovye prevrashcheniya i svoystva poluprovodnikovogo kremniya. Vysokochistye metallicheskie i poluprovodnikovye materialy. Kharkovskaya nauchnaya assambleya ISPM-8, 68–73.
42. Taran, Yu. M., Kutsova, V. Z., Nosko, O. A. (2002). Fazovi peretvorennia ta vlastyvosti napivprovidnykovoho kremniiu. Metaloznavstvo ta obrobka metaliv, 1–2, 59–65.
43. Taran, Yu. M., Kutsova, V. Z., Nosko, O. A. (2004). Semiconductor–Metal Phase Transitions. Uspehi Fiziki Metallov, 5 (1), 87–166. https://doi.org/10.15407/ufm.05.01.087
44. Kutsova, V. Z., Stetsenko, A. P., Mazochuk, V. F. (2017). Phase transformations in semiconductor silicon by the influence of magnetic field. Systemni tekhnolohii. Rehionalnyi mizhvuzivskyi zbirnyk naukovykh prats, 5 (112), 103–107.
45. Oranska, O. I., Gornikov, Yu. I., Gun'ko, V. M., Brichka, A. V. (2022). On the use of model diffraction profiles in the microstructure analysis of nanocrystalline metal oxides based on powder x-ray diffraction data. SURFACE, 14 (29), 148–158. https://doi.org/10.15407/surface.2022.14.148
46. Makara, V. A., Vasiliev, M. O., Steblenko, L. P., Koplak, O. V., Kuryliuk, A. M., Kobzar, Yu. L., Naumenko, S. M. (2009). Influence of Magnetic Treatment on the Microhardness and Surface Layers Structure of Silicon Crystals. Physics and Chemistry of Solid State, 10 (1), 193–198.
47. Nosko, O. A. (2006). Osobennosti struktury, fazovye prevrashcheniya legirovannogo kremniya i modifitsirovannykh zaevtekticheskikh siluminov i razrabotka sposobov povysheniya ikh svoystv [PhD dissertation]. Dnepropetrovsk, Ukraine.
48. Kutsova, V. Z. (1993). Teoriya i praktika upravleniya strukturoy i svoystvami liteynykh splavov na osnove alyuminiya i titana [Doctor's thesis]. Dnepropetrovsk, Ukraine.

Edited by
Tetyana Baydyk

ENERGY SYSTEMS AND RESOURCES: OPTIMISATION AND RATIONAL USE

Maksym Kovzel, Olga Nosko, Tetyana Baydyk, Masuma Mammadova, Ernst Kussul, Airam Curtidor, Yurii Sniezhkin, Zhanna Petrova, Vadym Paziuk, Viacheslav Mykhailyk, Tetiana Korinchevska, Kateryna Samoilenko, Igor Kozlov, Vyacheslav Kovalchuk, Viacheslav Miliev, Mykola Holovin, Serhii Vistiak, Olexiy Kozlov, Natalia Dunaievska, Taras Shchudlo, Ihor Beztsennyi, Dmytro Bondzyk, Yevhen Miroshnychenko

Collective monograph

Technical editor I. Prudius
Desktop publishing T. Serhiienko

TECHNOLOGY CENTER PC®
Published in December 2024
Enlisting the subject of publishing No. 4452 – 10.12.2012
Address: Shatylova dacha str., 4, Kharkiv, Ukraine, 61165
